STUDY OF AREA SELECTIVE DEPOSITION BY COMPETITIVE ADSORPTION

A Thesis

Presented to the Faculty of the Graduate School

of Cornell University

in Partial Fulfillment of the Requirements for the Degree of

M.S.

by

Pengyuan Zhao

August 2020

ABSTRACT

Moore's Law has been the guiding principle for semiconductor industry to scale down the device size. Consumers have been directly benefited from the ever developed technologies that lead to a faster, smaller, and more reliable performance. In order to preserve the advantages inherited from "scaling-down", researchers have invested into "bottom-up" approach which extends the "leeway" before Moore's postulation reaches saturation.

Area-selective deposition (ASD) is an advanced technique to realize bottom-up fabrication as the device feature size shrinks to sub-5 nm scale. On the other hands, conventional top-down process, such as patterning of the substrate followed by selective etching process, tends to result misalignment errors. We have developed a proof-of-concept approach to address the challenge. The approach involves chemical vapor deposition (CVD) in which substrates are exposed to a precursor and a co-reactant. A third reactant termed "co-adsorbate" was utilized to direct growth only occurs on one surface in the presence of another. In this work, 4-octyne was used as co-adsorbate in the CVD of ZrO_2 thin films on SiO_2 and Cu substrates. Expected from quantum chemistry calculation, 4-octyne favors binding on Cu substrate through rehybridization, whereas it only interacts with SiO_2 by van der Waals force. The difference in binding energies affords selective growth.

BIOGRAPHICAL SKETCH

Pengyuan Zhao was born in a rural area in north part of China. As the first-generation college student in the family, Peng decided to pursue a higher education that challenges the norms and embraces the truth. After declining the offer from a top Chinese university, he entered Matlock Academy in West Palm Beach, FL, as a senior high school student. Fascinated by watching the NASA launching of Expedition 38 in 2013, he decided to pursue a degree in Engineering discipline. Upon graduation in 2014, he entered Purdue University and claimed chemical engineering as the major. Throughout the four years at Purdue, Peng honed on his academic performance and research experience. To further exploit the benefits of "exploring the world", he exchanged the full semester at The University of Queensland in Australia in 2017. And in 2018, he graduated from Purdue with cum laude.

The journey of exploring proceeded. He joined Engstrom's research group at Cornell University in November 2018. Under the guidance of Prof. James Engstrom, he studied the cutting-edge technologies for semiconductor fabrication. Working in a group with everyone from different cultural background, Peng established broaden view towards the concept of "citizen of the world", one of the long-term goals that he wishes to achieve, upon completing the study in the United States. After graduating from Cornell, he is ready to start the career at ASM America, as a process engineer.

ACKNOWLEDGEMENTS

First, I want to express my deepest gratitude to my parents, Shengjun and Lijuan. They have been decisive and supportive for every decision I made in the past 25 years. Life is hardly rewarding without their confidence in me.

I want to thank Prof. James Engstrom, for granting me the valuable opportunity to study a new subject, his supervision and guidance are important, without which it would be difficult to endorse my ability at a prestigious company in the semiconductor industry.

In addition, I want to thank all my colleagues at Engstrom research group, for their seamless assistance during my stay. In particular, I want to thank Taewon Suh, for his step-by-step guidance to help me enter a new field. Taewon has been my everyday colleague in the lab, in which he taught me many applications including running ultra-high-vacuum system, X-ray Photoelectron Spectroscopy, mass spectroscopy, etc. His patience and the good will to help the next-generation are greatly appreciated.

TABLE OF CONTENTS

LIST OF TABLES

LIST OF FIGURES

CHAPTER 1

INTRODUCTIONS

1.1 Background and Motivation

1.1.1 Semiconductor Industry

In 1965, the co-founder of Intel Gordon Moore predicted that the number of transistors in a unit microchip doubles every two years, known as ”Moore’s Law” (Figure 1.1). For decades, this postulation has been the driving force for the semiconductor industry to pursue device scaling. Industries aim to scale-down the device to obtain smaller size and faster performance. Consumers are therefore able to purchase more advanced laptops and cell phones in reduced prices. Today, however, the progress that reflects ”Moore’s Law” is foreseen to reach saturation. In order to preserve the benefits of ”scaling”, many applications now favor more complex structures. In particular, three-dimensional (3D) chips are predicted to keep Moore’s law alive [1]. 3D integration has been employed in many areas such as fuel cells [2], chemical sensors [3], and 3D photonic crystals [4]. Traditionally, 3D structures are fabricated using 2D patterning techniques such as photolithography followed by etching or lift-off, which the device performance can be hindered by the sophisticated ”top-down” process.

Area-selective deposition (ASD) is a ”bottom-up” solution to 3D structures that thin films are deposited uniformly at the desired region. This thesis will begin by reviewing two important deposition techniques, chemical vapor deposition (CVD) and atomic layer deposition (ALD), then focus on developing our

proof-of-concept approach to area selective deposition using modified CVD.

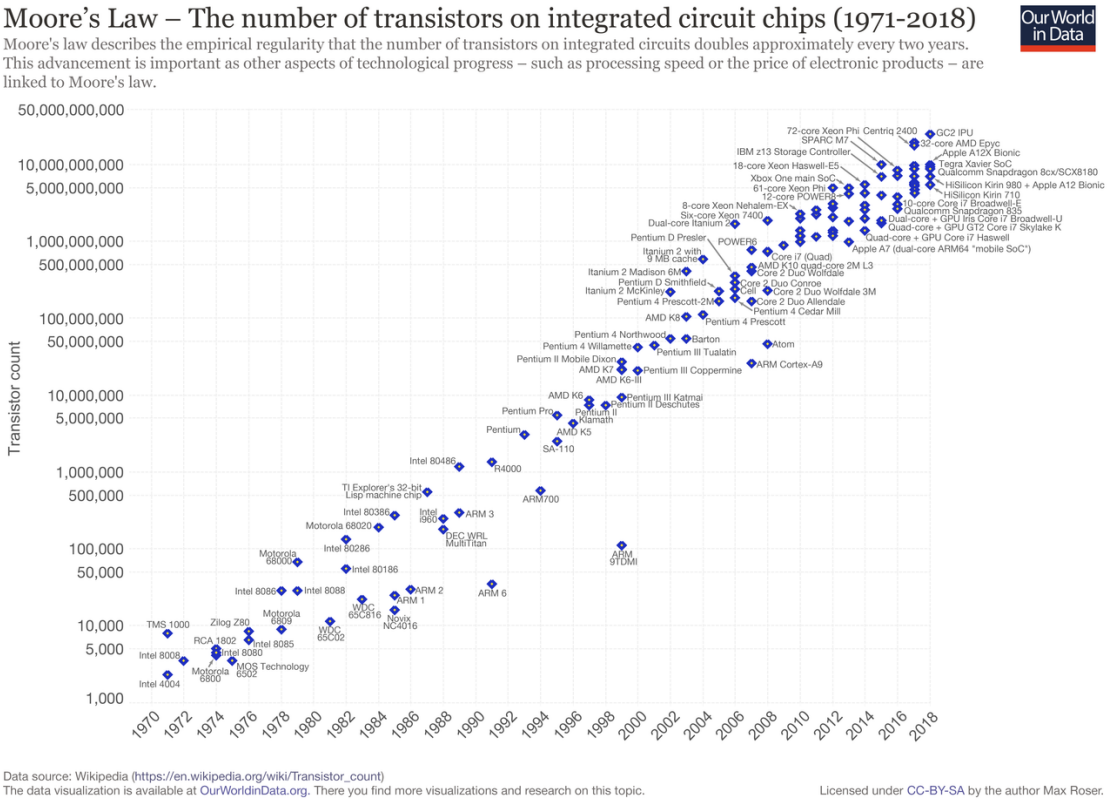

Figure 1.1: Moore's Law, number of transistors on a integrated circuit chips (1971 - 2018)

1.1.2 CVD and ALD

Chemical vapor deposition (CVD) is a chemical process in which gaseous precursor reacts with co-reactant to form nonvolatile products that are deposited at the substrate surface. CVD has been extensively used for coatings of airplane engine, production of thin film for microelectronic devices, and more recently used to fabricate graphene, which shows promising future for photovoltaic cells and field effect transistors [5]. Owing to its compatibility, many versions of CVD have been developed, such as atmospheric pressure (APCVD),

low pressure (LPCVD), plasma-enhanced (PECVD). Modified CVD processes are adapted to resonate process requirement, specifically, the need for reduced ambient pressure as well as overcoming energy barriers. Nevertheless, a fundamental CVD includes the following steps: 1) transport of gaseous reactants to the reaction zone; 2) adsorption (physical or chemical) of the reactive species on the substrate surface; 3) chemical reaction catalyzed by the surface to form nonvolatile products; 4) desorption of reactive species and purge of the reaction by-products. Figure 1.2 illustrates the difference between a standard CVD versus the modified CVD, which the latter was used to afford area selective deposition. The unique part of our modified CVD process is it includes a third species termed co-adsorbate, which is a small molecule that help prevent thin films from growing on undesired regions, therefore, leading to selective growth.

Atomic layer deposition (ALD) is another technique that can deposit thin films produced from various vapor phase materials. ALD also features chemical reaction at the substrate surface. In fact, many ALD processes are derived from their CVD counterparts[6]. As the device design continues to shift toward three dimensional, a more rigorous and precise approach is demanded to deposit uniform thin film at these complex structures. ALD is capable of meeting this need thanks to the nature of self-limiting and sequential exposure. A general ALD process is shown in Figure 1.4. Starting from a bare substrate, the precursor is first pulsed in to chemisorb onto the substrate surface (i.e. occupy the available binding sites). The process is called a ”half-reaction”, which leaves no more than a monolayer of the chemisorbed precursor at the surface (self-limiting). When the binding sites are saturated, inert gas (N_2 or Ar) is pulsed in to purge out excess precursor molecule. During the second ”half-reaction”,

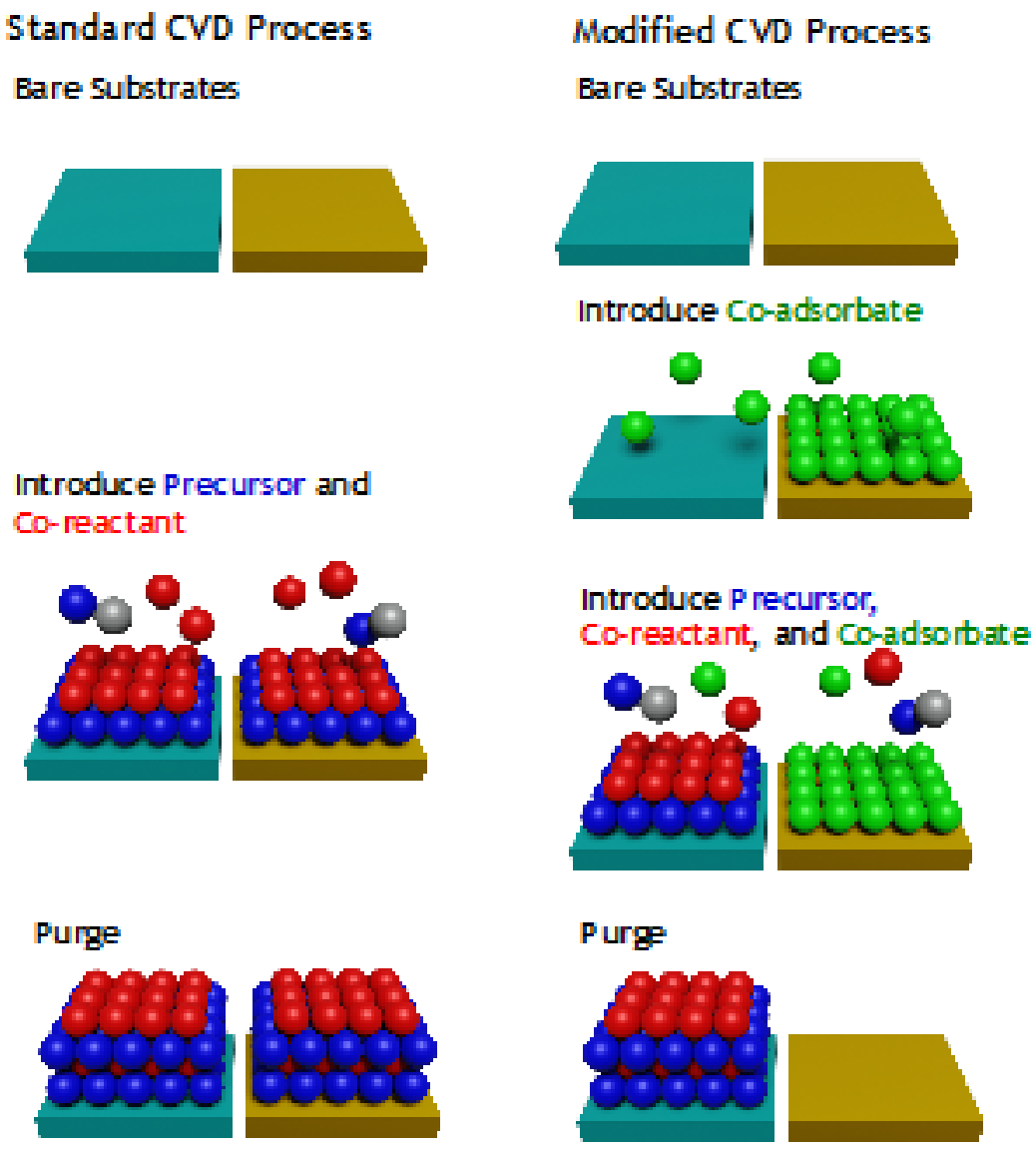

Figure 1.2: Standard and Modified CVD

co-reactant (O_2 or H_2O) is pulsed in to react with the precursor that forms up to a monolayer of the growth material (sequential exposure). Another purge of inert gas is introduced to remove any volatile by-products and unreacted materials, leaving a new starting surface for the next ALD cycle. The cycles are then repeated several times until desired thickness of the material is achieved. Compared to CVD which generally conducted at high temperature (> 600 °C),

ALD is usually conducted at moderate temperature (< 350 °C , which is known as ALD "temperature window"[6]). Each ALD process has the unique temperature range in which saturation behaviors can be expected. Outside this window, ALD process tends to result in poor film growth due to thermodynamics such as slowed reaction kinetics (low temperature) or precursor decomposition (high temperature).

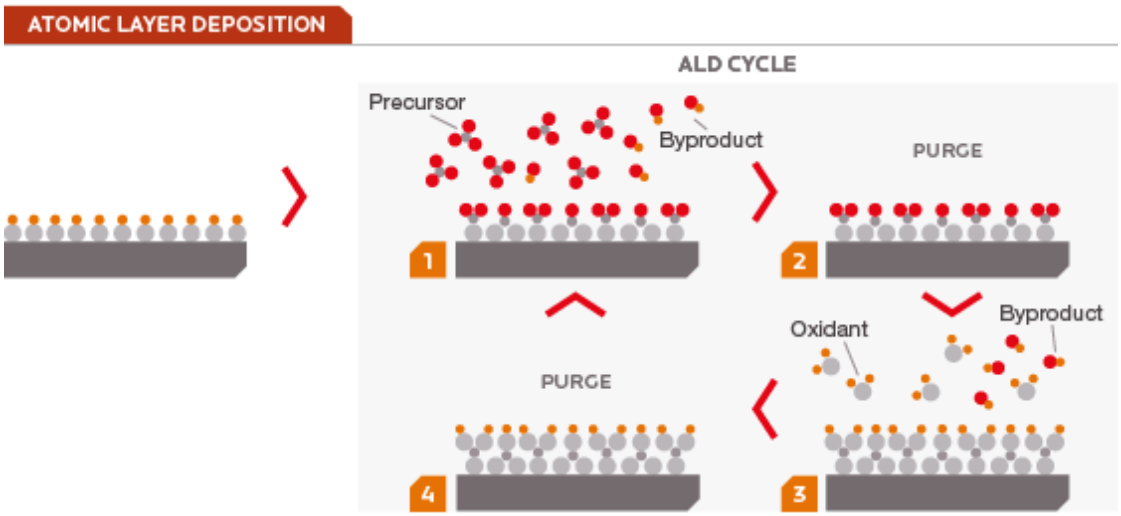

Figure 1.3: Standard ALD process, courtesy of ASM International[7]

It is foreseeable that ALD is able to produce a uniform thin film with the self-limiting nature, given right thermodynamics and transport conditions. Additionally, the layer-by-layer growth nature allows for precise thickness control of the thin film. Pore *et al.* deposited a phase change material germanium antimony telluride (GST) by ALD in a highly controlled manner[8]. Given sufficient time, the alkylsilyl precursors travel into the high-aspect ratio trenches, fully react with the surface, and leave uniform coverage. The cyclic pulses of co-reactant and precursors allow the thin film to grow in a controlled rate, called growth per cycle (GPC), which is typically less than 1 angstrom/cycle. The researchers were able to grow the GST film at 0.6 Å/cycle and the SEM image showed a high-aspect ratio structure covered with uniform GST film.

Despite the fact that ALD is more practical concerning area selective deposition, CVD process was chosen for this study to demonstrate the feasibility of competitive adsorption. The modified CVD process is able to examine the surface chemistry more efficiently than using ALD. CVD is preferred since it is easy to execute, considering the objectives involve investigating a process window for this competitive adsorption mechanism. Moreover, CVD can be conducted at relatively high temperature such that the reversibility of the adsorption can be studied. Nonetheless, a CVD process that includes a third species will introduce as many as nine interactions (Figure 1.3) that must be carefully evaluated. For example, an ideal co-adsorbate candidate should not directly react with the precursor molecules, either being transported in vapor phase or upon adsorbing on the substrate. Hence, it is important to consider the molecular structure of the co-adsorbate, which in turn controls the reactivity towards both precursor and substrates.

1.2 Area Selective Deposition (ASD)

1.2.1 Inherent Selective Deposition

Inherent selective deposition is a straightforward route to realize selective growth, taking advantage of the intrinsic reactivity differences due to varied substrates or precursor chemistry. Green *et al* compared growth of HfO_2 films on hydrogen terminated Si and chemical oxide substrate[9]. They found that growth on the former results in a large nucleation barrier while the growth on oxide is characterized by almost no barrier. The ease of nucleation on oxide is

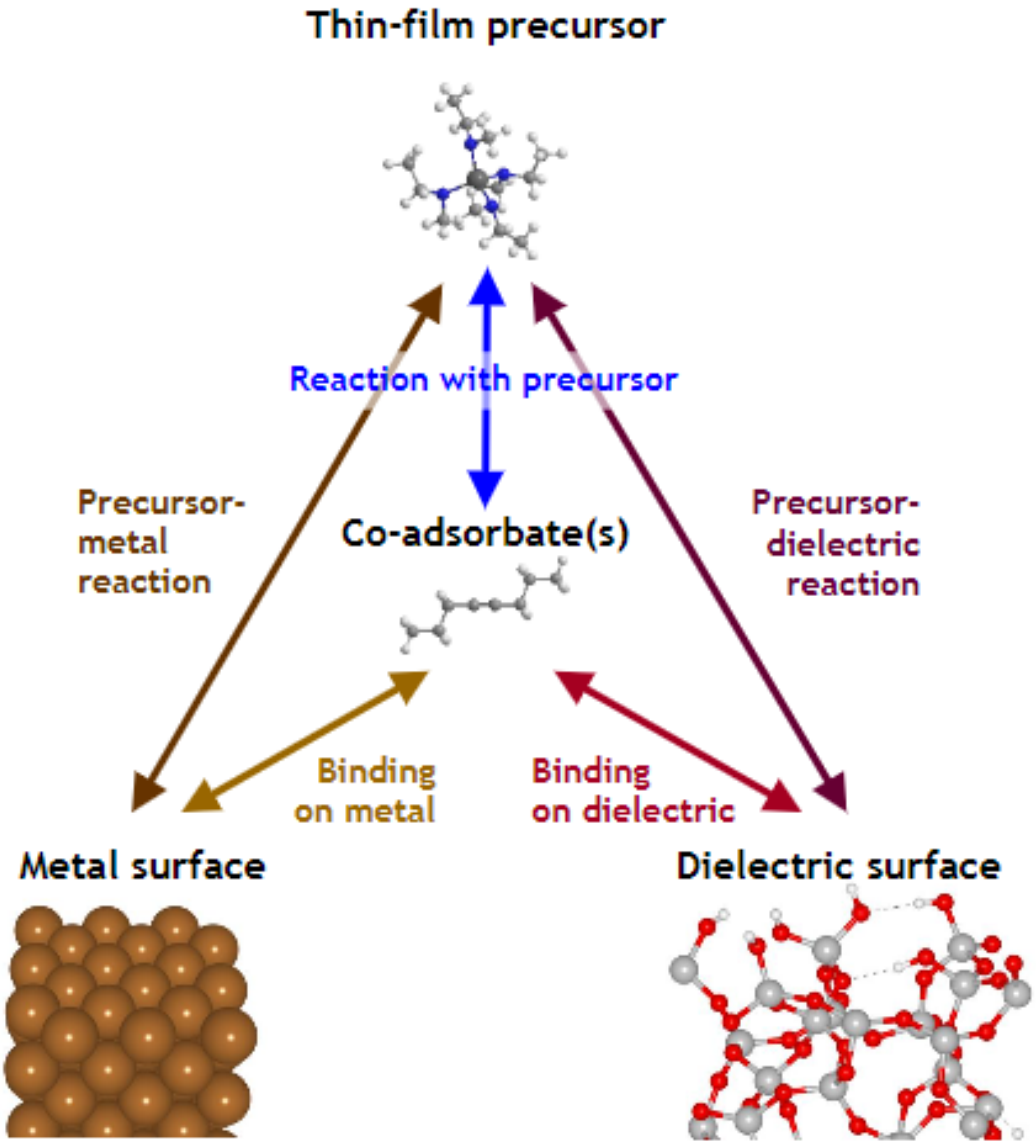

Figure 1.4: Interactions in CVD involving a third species, interactions by co-reactant are not included

due to great concentration of hydrous OH group on the layer that favors precursor adsorption. To confirm that favorable nucleation occurs on oxidized surface is due to the enriched OH groups, McDonnell *et al.* reported different nucleation results of TiO_2 film growth on hydrogen terminated Si and oxidized Si surfaces [10]. It was found that OH coverage favors loss of precursor ligands which fa-

cilitates the nucleation process. The results further pronounce the possibilities of achieving selective growth just by inherent selectivity. However, the lack of versatility is a major concern. Finding the combinations of substrates that afford perfect selective growth remain a challenge. Furthermore, the selectivity is restricted by the initial nucleation delays on substrates[11]. Although selective for the initial stage, the process' lack of durability when significant nucleation took place on the non-growth region made the net result non-selective. One can appreciate the fact that intrinsic selectivity is the precursor to a successful ASD, yet it alone is not enough to sustain the selectivity.

1.2.2 Atomic Layer Etching

Atomic layer etching (ALE) can be viewed as the inverse of ALD, in which the step etches away materials that are already deposited on the undesired region. Similar to ALD, ALE can also be controlled at the atomic level. ALE has been integrated into conventional ALD cycles to afford selective growth. Typically, an ALE cycle is coupled with numbers of ALD cycles to achieve net area selective deposition. Mackus *et al.* studied area selective deposition of ruthenium on Pt/SiO_2 patterned substrate[12]. Apart from general ALD steps, an etch step was added for every 100 ALD cycles, which introduces O_2 plasma for 20 s to remove Ru on non-growth region. It is known that O_2 or O_3 plasma reacts with Ru and form RuO_4 which is a volatile byproduct that can be easily removed. The SEM image shows ruthenium only grew on Pt regions in the presence of SiO_2 surface with the treatment of etching. ALE can also signify the selectivity by extending the nucleation delay between two substrates. In the PEALD process to deposit Ta_2O_5 thin film, Vallat *et al.* used oxygen plasma mixed with small

amount of NF_3 to etch the thin film on Si/SiO_2 surface substrate. The idea of adding NF_3 is not only to selectively remove thin film layers, but also to passivate the Si/SiO_2 by forming Si-F or SiO-F bonds, which subsequently created a new nucleation delay for the next ALD cycle[11]. Figure 1.5 illustrated the idea, which shows that selective thickness by ALD + ALE is greater than that of ALD alone, and the difference is enhanced by the nucleation delay regenerated after each ALE cycle. It seems that ALD integrated with ALE is a plausible solution to area selective deposition, however, there are a few considerations.

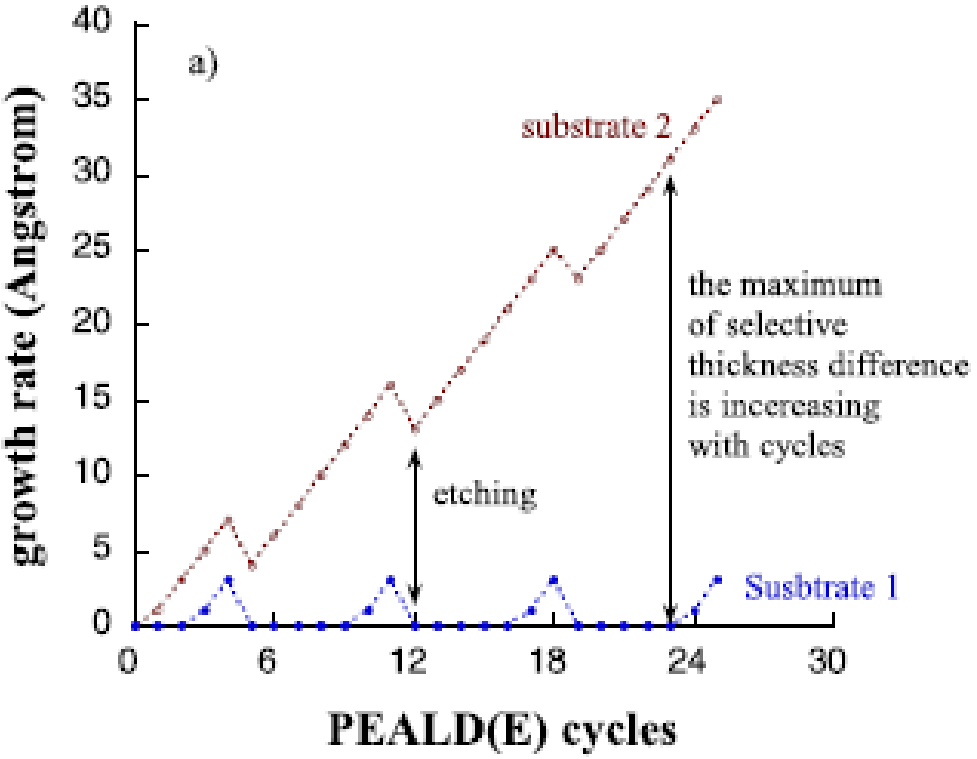

Figure 1.5: Illustration of extended nucleation delay caused by adding ALE step, Vallat *et. al*, 2017 [11].

First, there must be reactivity difference towards etching, or it proceeds with no contrasting rates on both surfaces, eventually leading to non-selective

growth. The etchant used in the ALE cycle should not remain on the surface or be incorporated into the deposited films. Song *et al.* designed "30/5 ALD/ALE supercycles" to deposit TiO_2 selectively on SiO_2 in the presence of Si-H surface. For every 30 ALD cycles ($TiCl_4$ and H_2O), 5 ALE cycles (WF_6 and BCl_3) were added to remove the grown film. However, the deposited TiO_2 film contained 3-5 at.% boron and 1-2 at.% fluorine[13]. In the previous ruthenium ALE study by Mackus, exposing Ru to oxygen plasma will oxidize the surface, therefore a post H_2 exposure has to be added. Additionally, long processing time for a complete ALD/ALE cycle remains a challenge. The total deposition time for one supercyle in TiO_2 ALD takes about 50 min[13], the throughput needs to be improved to address the demands from the industrial sector.

1.2.3 Self Assembled Monolayers (SAMs)

Self Assembled Monolayers (SAMs) are organic monolayers that can tune the reactivity at the substrate surface. SAM is a group of alkyl chained molecules that consist of a tail group and a reactive headgroup. SAMs are particularly useful to direct thin film growth if the key functional groups in the layers are carefully designed. They can block the active binding sites at the substrate thus preventing precursors to adsorb on the surface. Similar to previous ASDs, one has to design a SAM that has intrinsic differences in affinities towards different substrates and the tail groups should not react with the precursors.

Yan *et al.* studied atomic layer epitaxy growth of ZnO on substrates that are lithography-patterned with SAMs[14]. Crystalline ZnO layers selectively grow on surface that is not covered by SAMs. The SAMs are poly(dimethylsiloxane)

(PDMS) that consist of patterned arrays fabricated from a Si master. The layers are transferred on Si substrate to form a patterned substrate with growth region exposed. On the non-growth region, the headgroup of the SAM reacts rapidly with the surface hydroxyl groups on Si and the hydrophobic tail structures form densely packed monolayers. Using this method, the group demonstrated 60 nm of ZnO was deposited on the regions not covered by SAMs. The growth region had sharp edges and the SAMs were free of Zn, suggesting SAMs is a promising way to realize area selective deposition.

However, there are some drawbacks associated with SAMs. One of the major challenges is that the blocking ability is heavily dependent on the quality of the SAMs. Jiang and Bent studied extensively on area selective deposition using SAMs. They found that the chain length, tail group, headgroup, and the SAM formation time all affect SAM properties[15]. For example, the blocking ability was found to drop with shorter chain length. In order to sufficiently block HfO_2 growth on SAM-covered region, the alkyl chain lengths must be greater than 18 units of carbon[15]. The densely packed monolayers require hours of preparation. In their HfO_2 ALD study, the preparation time for an octadecyltrichlorosilane (ODTS)-coated Si wafer took over 40 hours. Moreover, it is difficult to fabricate defect-free SAMs. Hua *et al.* used a heated AFM cantilever probe tip to pattern a polymethyl methacrylate (PMMA) SAM [16]. The SAM layer, upon thermally modified, created a residual layer that was about 5 nm thick. Even the residue layer was shown to be removed by O_2 plasma, it introduced additional steps which are not efficient in terms of mass industrial production scaling.

1.2.4 Competitive Adsorption

Use of a third species to direct thin film growth on specific region has become another proof-of-concept approach to achieve area selective deposition [17, 18, 19]. There are three general mechanisms concerning this approach. The third species, termed co-adsorbate, can be used as a site-blocking agent to block precursor nucleation on specific region. It may also modify the surface reactivity by tuning the functional groups at the surface. Moreover, it may recombine with chemisorbed precursor, a reversible process to regenerate the reactive species, thus delaying the nucleation process. Nonetheless, a generic approach to ASD likely to involve one or more aforementioned mechanisms.

Mameli *et al.* and co-workers employed a "ABC" cycle to achieve area selective deposition, which comprises acetylacetone (Hacac) inhibitor (A), bis(diethylamino)silane (BDEAS) precursor (B), and oxygen plasma coreactant (C) [17]. The process was carried out on a patterned Al_2O_3/GeO_2 substrate aiming to grow SiO_2 selectively on GeO_2 region. The Hacac inhibitor prefers to bind on Al_2O_3 surface and block the BDEAS precursor molecules from chemisorbing (step A). Upon the BDEAS precursor saturates on the GeO_2 surface (step B), the adsorbed Hacac inhibitors are removed by oxygen plasma pulse (step C), and the surfaces are ready for the next ABC cycle. Using this approach, 0.01 nm thick SiO_2 layer was able to grow exclusively on GeO_2 substrate after 15 ALD cycles. Though the growth rate was kept very low, because the additional etching step did remove some amount of the thin film on the growth region, it is a clear example of using a third species to block thin film growth. The process is entirely in vapor phase which reduces the complexity of introducing chemicals to the system and is easier to be integrated with current ALD technique.

On the other hand, mohimi *et al.* used ammonia to inhibit nucleation on oxide surfaces in the CVD of metallic film deposition[18]. In addition to metal carbonyl precursors, the researchers added an ammonia coflow and found significant nucleation delays occurred on oxide surfaces but not on titanium metal or vanadium nitride substrates, suggesting the reactivity difference on the substrates that benefits the early stage of ASD. In contrast to the site blocking mechanism, the ammonia added in the process worked by creating a condition that disfavors decarbonylation of the adsorbed metal carbonyl intermediates, a process that forms the final product - metallic film. There are two possible explanations, ammonia can either bind with surface hydroxyl groups thus reducing the acidity of the oxide surfaces that disfavors precursor nucleation, or it can directly bond to the metal center to stabilize the carbonyl intermediates from conversion to metal nuclei. However, this study did not use a co-reactant, instead, NH_3 worked as a co-reactant considering significant incorporation of nitrogen in the film. This approach, while pronounced the benefits of competitive adsorption, diminishes the idea of using competitive adsorption as a flexible approach that can accommodate vast process variable selections, including the choice of a co-reactant.

Competitive adsorption in this thesis employed a similar idea to use a third species to suppress thin film growth in specific region. The major differences to other methods are: (a) it intentionally introduces co-adsorbate and precursors together; (b) co-reactant is included which is standard in ALD/CVD process; (c) the process is entirely in vapor phase, which reduces the complexity of process integration.

No matter which route to area selective deposition, attention has to be paid

to the interactions induced by the process, particularly by the newly added species. The intrinsic selectivity between two starting substrates need to be significant in order for co-adsorbate to bind preferably on one in the presence of another. Concerning the co-adsorbate, the adsorbed molecules should be able to delay or suppress thin film growth. Plus, the adsorbed co-adsorbate should desorb from the surface in the subsequent steps to avoid being incorporated in the film. To promote competitive adsorption, co-adsorbate is introduced during the entire course of experiment. Therefore, it should be cautious to minimize the potential side reaction between the co-adsorbate and precursor in the vapor phase.

The major objective of this study is to develop a generic approach for area selective deposition. Specifically, the process involves depositing thin film layers of ZrO_2 on SiO_2 (dielectric) in the presence of Cu (metal) by CVD. Undoubtedly, one could argue that many degrees of freedom in this process makes it challenging to become a proof-of-concept approach. Inherent selectivity between substrates, choice of suitable co-adsorbate candidate, and proper thermodynamics, all contribute to successful ASD by competitive adsorption. Nonetheless, evidencing the adaptability is not equal to tuning all the process variables at the same time. For example, the dielectric material deposited on dielectric substrate (DoD) constitutes a common "bottom-up" step employed in the process of field-effect transistor (FET) fabrication, which already surpassed some "top-down" processes in terms of produced film qualities. With the generic approach developed, one can further exploit the benefits of competitive adsorption by tuning the process variables to satisfy particular demands. The versatility can be demonstrated by switching combinations of substrates, exploring the bindings of different co-adsorbate molecules, changing to ALD instead of CVD, and even

reversing the selectivity to deposit thin film on metal (DoM). In fact, surface chemistry on cobalt was studied as the first step to investigate the feasibility of changing substrates. The results sections will address the current state of the aforementioned issues on which the future work can be extended based.

CHAPTER 2

EXPERIMENTAL SETUP

2.1 Materials

Materials used to investigate competitive adsorption include precursor, co-reactant, and co-adsorbate. The precursor used in the study is Tetrakis(ethylmethylamido)zirconium (IV) $Zr[N(CH_3)(CH_2CH_3)]_4$,TEMAZ (Figure 2.1) (99.9999%, Air Liquide). Co-reactant used is molecular oxygen (UHP, Airgas). Co-adsorbate used in the experiment is 4-octyne (Sigma-Aldrich, 99%). The precursor and co-adsorbate are in liquid phase and stored in stainless steel bubblers, and the oxygen is stored in gas cylinder. Due to its flammable nature, TEMAZ is loaded into the bubbler inside a glove box located at Cornell Center for Materials Research (CCMR). Reactants are delivered to the microreactor through separate carrier lines to minimize side reactions in the gas phase.

2.2 Ultra High Vacuum Chamber Setup

The experiments are conducted in a customized Ultra High Vacuum (UHV) chamber. The UHV system consists of four major sections, a loadlock chamber, a microreactor, an intermedite chamber, and a main analysis chamber (Figure 2.2). A sample manipulator (Thermionics SMR-3, Thermionic Northwest, Port Townsend, WA) is installed to transport the sample inside the UHV chambers. The sample manipulator allows movement of sample in x,y,z direction, it also allows polar and azimuthal movements. To prevent any unwanted air leak

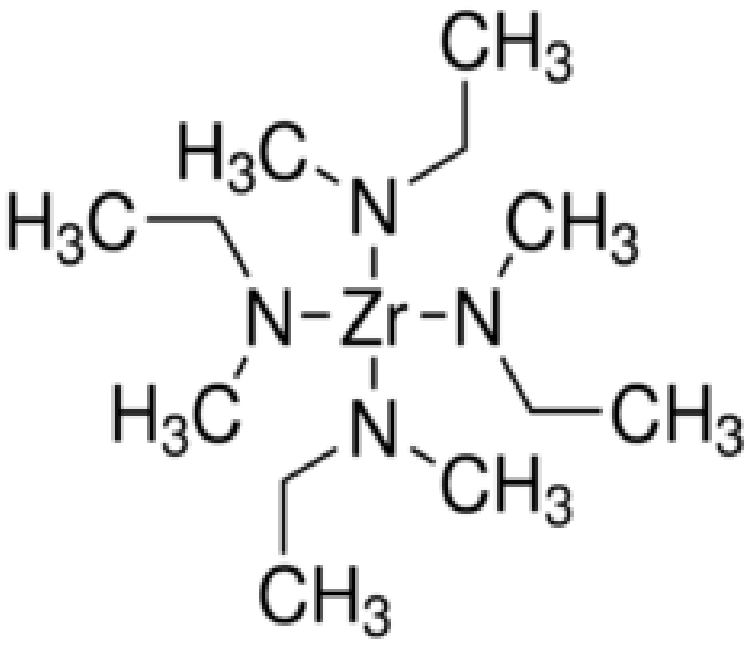

Figure 2.1: TEMAZ, reprinted from Sigma-Aldrich

during polar and azimuthal movements, a differential seal is created within the sample manipulator assembly. The inner section is pumped by an ion pump (Ion Pak 200, Perkin-Elmer Products, Waltham, MA) and maintained at ultra high vacuum. The outer section is pumped by a mechanical pump and maintained at 10^{-2} Torr.

Coupon samples are housed in a sample holder. The holder is made of molybdenum and can be customized to hold different shapes of sample. In this experiment, the sample holder has two identical recess regions that can hold two 10 x 25 mm^{-2} rectangular samples. The holder design allows to examine two different materials upon exposure to chemicals at the same time. Samples housed in the sample holder can be heated by pyrolytic boron nitride heating element installed at the back of the holder. Temperature calibration was done by previous group members to control the substrate temperature accurately.

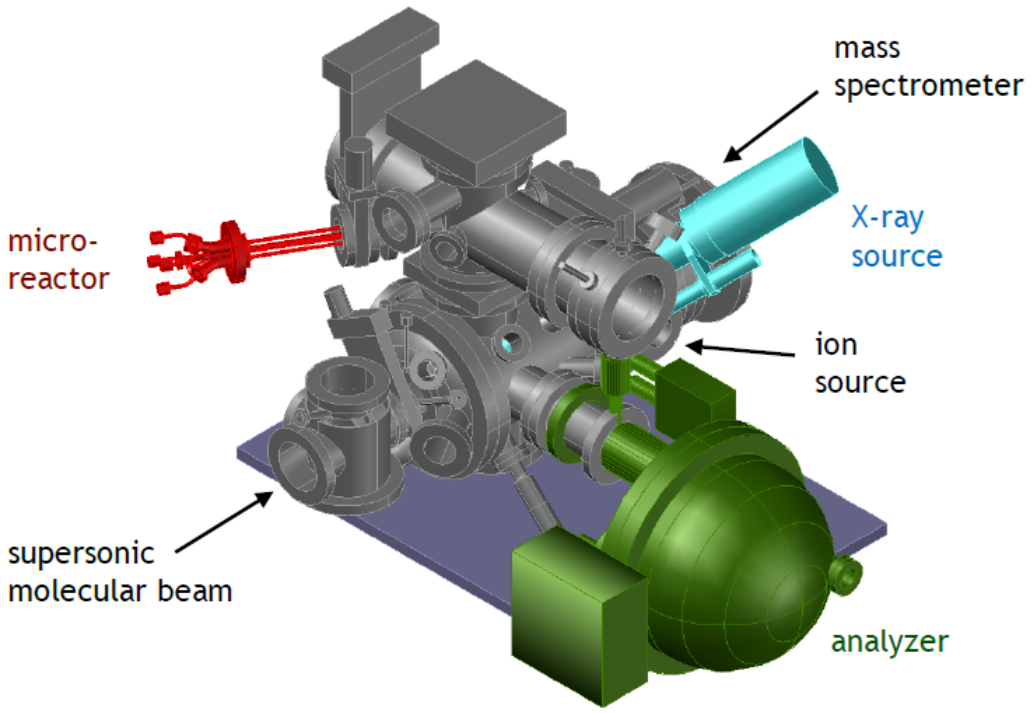

Figure 2.2: Schematic of the UHV chamber, loadlock, sample manipulator, and sample holder are not shown, Chen, 2017 [20].

Loadlock chamber is designed to have sample loaded without having to break the UHV condition for other parts of the system. To load samples, rectangular coupon samples are first slid into the recess regions on the sample holder. With loadlock chamber vented to atmosphere, the sample holder is hooked onto a transfer arm that can be extended horizontally inside loadlock chamber. A designated person performs the job wearing web coat and gloves to minimize any surface contamination. Once the holder is secured on the transfer arm, the chamber surface is wiped with isopropylcohol (IPA) or acetone to minimize contamination. The loadlock door is then shut and the chamber is pumped down by a turbomolecular pump (Pfeiffer TMU 071 P) to high vacuum. When 5.0 x 10^{-6} Torr of pressure is reached, the ion gauge is turned on to reflect real-time loadlock pressure.

The intermediate chamber is a connection between the other chambers. When the pressure in the loadlock is reduced to sufficiently low of 1×10^{-7} Torr, the gate valve connecting loadlock and intermediate chamber is open. The transfer arm carrying the sample holder are approached to a close contact with the receptor inside the intermediate chamber. Sample holder is then locked onto the sample manipulator through reverse mechanism of loading. In the course of an experiment, the intermediate chamber is open to connect with the reactor through microreactor probes. When sample transfers down into the main analysis chamber, the main gate valve is open to allow the sample to be transferred *in vacuo*. After each experiment, comparable pressure level needs to be established between intermediate chamber and main chamber for post-exposure analysis. To accomplish this, the reactor gate valve is closed, leaving the intermediate chamber a closed volume. The excess gaseous reactants are directed to the main chamber by a bypass valve and pumped away by the ante turbomolecular pump (Pfeiffer TPU 261 PC). The main gate valve is open to the intermediate chamber when the pressures in these two volumes reach comparable level, by monitoring the foreline pressure of the ante chamber no longer changes.

Main chamber is pumped by a turbomolecular pump (Osaka TG 403M) and maintained at a base pressure of 1×10^{-9} Torr. Main chamber houses surface characterization tools for post-exposure analysis. A concentric hemispherical analyzer and a Mg/Al twin anode X-ray source are installed for X-ray Photoelectronic Spectroscopy (XPS). A quadruple mass spectrometer (QMS, Hiden 3F/EPIC, Hiden Analytical, Warrington, UK) is used to carry out Residual Gas Analysis (RGA). RGA detects signals for mass to charge (M/Z) ratio from 1 to 300, an important technique to identify and quantify elements inside the chamber. In the event of an air leak, QMS is employed to quantify M/Z ratio of

18(H_2O), 28 (N_2), and 32 (O_2) for the presence of contaminants. The main chamber is also capable of doing low-energy ion scattering spectroscopy (LEISS). Although not directly employed in this study, the ion source for LEISS can generate argon ions to sputter substrate surface. Argon ion sputtering is frequently used to prepare a clean substrate surface. When combined with XPS, a sputter-depth profile can be generated to characterize the film.

2.3 Microreactor Setup

Previous group member and co-workers designed a microreactor for thin-film deposition[20]. One of the merits using this microreactor setup is it forms a confined reaction zone where it is isolated from surrounding environments. In the course of the deposition, precursors and carrier gases can enter and exit the reactor through individual feedthroughs, thus minimizing crossed contamination and potential side reactions in the vapor phase. Computational Fluid Dynamics (CFD) simulation was employed to optimize the transport phenomena inside the reactor. The final design yields a reaction zone equivalent to 1 cm^3.

The microreactor assembly has five fluidic feedthroughs for gas deliveries, three of them are for gas inlets and two are for effluents (Figure 2.3). Before deposition, the microreactor head is approached into the intermediate chamber and comes to a physical contact with the sample holder. The cylindrical reaction zone is established by the central fluidic extension, two surrounding effluent lines, and the substrate surfaces. There are four electrical feedthroughs (not shown) on the mounting flanges that can be used for continuity check. During deposition, each gas species is introduced separately to the reaction zone and

any excess will be purged through the effluent lines by the mechanical pump. The reactor pressure during deposition is regulated to be at 1.5 Torr, which is controlled by a capacitance manometer combined with a throttle valve.

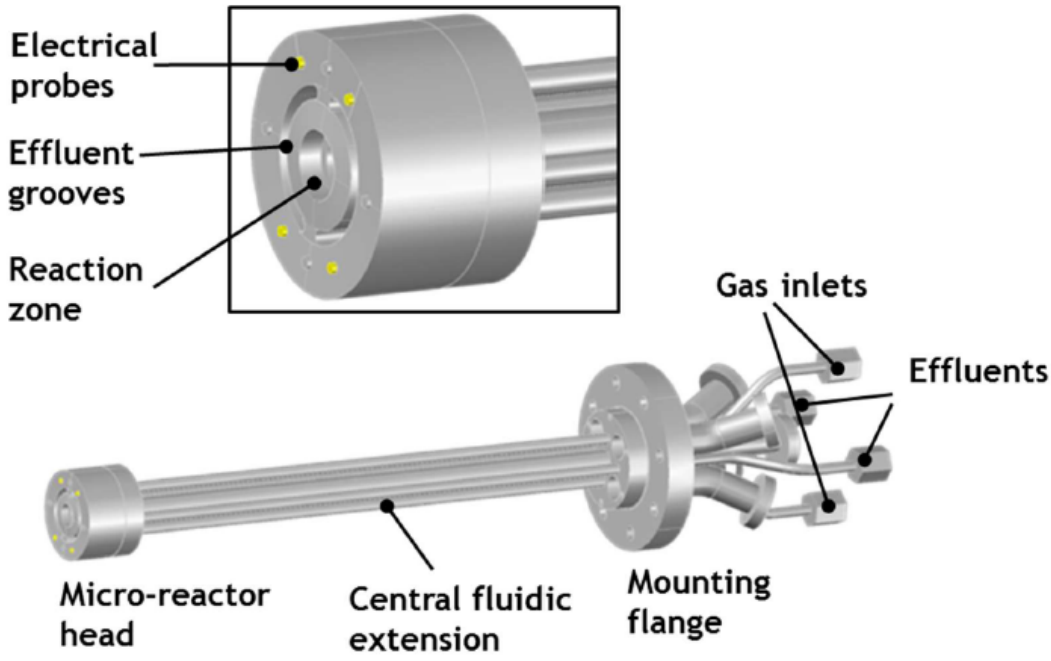

Figure 2.3: Schematic of the microreactor assembly, Chen, 2017 [20].

2.4 Delivery System

The delivery system uses a sliding panel assembly that includes several parts for gas delivery. There are three individual panels (A,B,C) machined on the moving stand. Figure 2.4 illustrates the components on a single panel[21]. Each panel includes separate delivery channels for carrier gas and purge line. Nitrogen (HP, Airgas) is used as carrier gas in the experiment. From the gas cylinder, the carrier gas flow rate (sccm) is controlled by mass flow controller (MKS Instruments, Andover, MA). TEMAZ and 4-octyne bubblers are located on the

carrier gas line A and C, respectively. To transport chemicals, the bubbler inlet has a dip-tube through which the carrier gas can reach into the precursor in liquid phase. Upon a phase equilibrium is reached, precursor molecules will be transported downstream through the bubbler outlet. The amount of vapor phase molecule in the carrier gas is proportional to its partial pressure. A water bath is set up to control the bubbler temperature.

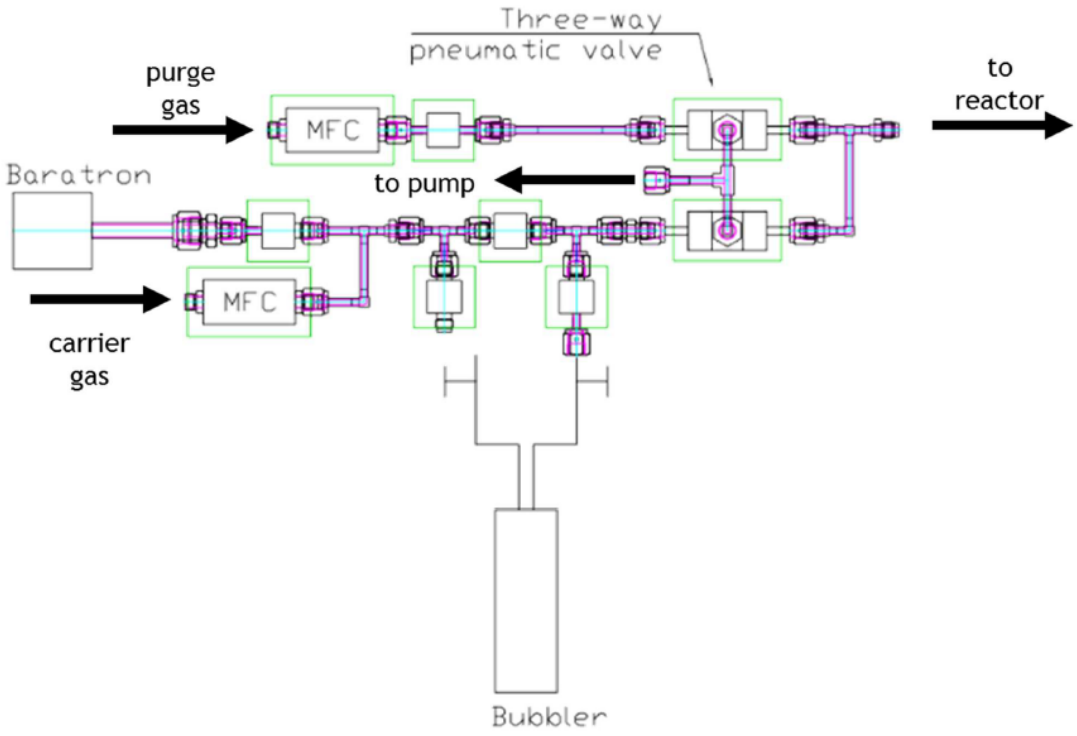

Figure 2.4: Schematic of the components on a delivery panel, Suh, 2017 [21].

A three-way pneumatic valve assembly is used to direct the flows to either the microreactor or mechanical pump. During a purge step, the purge lines are open to the reactor while the carrier gas lines are directed to the mechanical pump for exhaust. The pneumatic valves are controlled by Labview program. The program is capable of operating multiple valves at any given time. Combinations of valve open-close settings are manually input for each CVD step before experiment and executed automatically as experiment proceeds.

2.5 X-ray Photoelectron Spectroscopy

X-ray Photoelectron Spectroscopy (XPS) is a surface-sensitive analysis technique that can reveal elemental characteristics of a thin film. X-rays bombard the material surface and electrons from the atomic core levels are excited, which subsequently collected by an energy analyzer. XP spectra is obtained by constantly bombarding the surface while measuring the kinetic energy of the emitted electrons. Given the known X-ray photon energy, the binding energy (BE) of the electron in the solid can be calculated using the equation:

$$E_B = h\nu - E_K - \phi \tag{2.1}$$

where E_B is the characteristic binding energy, $h\nu$ is the energy of excitation, and E_K is the measured electron kinetic energy. ϕ is the work function of the material, which is equal to the energy difference between the Fermi level and the vacuum level. It accounts for the energy barrier that emitted electrons need to overcome at the surface. Since the calculated binding energies are characteristic for each element, the film composition can be revealed. In most cases, the calculated binding energies will differ from the reference by several eV, a term called "chemical shift", which caused by different oxidation state of the surface atom and the local chemical environment.

In 312, a twin-anode Mg/Al source (DAR 400, Omicron Nanotechnology, Eden Prairie, MN) is used to generate X-rays. The X-ray generation and XPS experiments are controlled using Omicron software. To acquire XP spectra, a survey scan is first conducted for the entire binding energy range (0 - 1000 ev). A detailed scan is followed for those elements in interest, which only scans over the binding energy regions where it shows the associated characteristic peaks.

For example, C-C single bond peaks at 284.8 eV, the scan range is set from 280 - 290 ev. XP spectra acquired are analyzed by Casa XPS software.

The XP spectra often contains many secondary structures such as X-ray satellite peaks and multiplet splitting due to complex chemical environment, therefore, it is crucial to obtain a precise background to quantify the major peak areas. Shirley method is used for background subtraction, in which the background intensity is always proportional to the intensity of the total peak area above the background[22]. The determination of the background using Shirley method requires iterative solution. To correct for "chemical shift" mentioned above, a core level peak of an element with known binding energy is selected, the difference between the binding energies are applied for all other elements with respect to that element. For example, "adventitious carbon" or carbon contamination on the sample is well known to be about 284.7 eV, if the measured carbon 1s peak is at 285.0 eV, a difference of +0.3 eV is applied to correct all peak positions for this specific analysis.

The XP spectra is also capable of quantifying surface atomic density and estimating film thickness provided a suitable reference [23]. The peak intensities from the spectra are proportional to the surface atomic concentration, which also depends on photoelectric cross-sections σ. Electrons emitted from the core will only travel a certain distance before attenuation, known as inelastic mean free path λ. Therefore, XPS is a surface-sensitive technique that the signal acquired only comes from the top 10 nm of analyzed film interface. To consider this attenuation effect, previous ERG group member Kevin Hughes developed four models that correlates attenuated photoelectron intensity as a function of take-off angle, as shown in Figure 2.5 [24]. A take-off angle is defined as the

angle between the direction in which photoelectron travels and the surface normal. For a substrate buried with thin film (the third model), one can obtain XP spectra at different angles and estimate the distance that photoelectrons travel to reach vacuum interface d, or the thin film thickness. Use of the models assumes that the inelastic mean free path λ does not vary with position, and the attenuation effect is only in the normal direction to the surface.

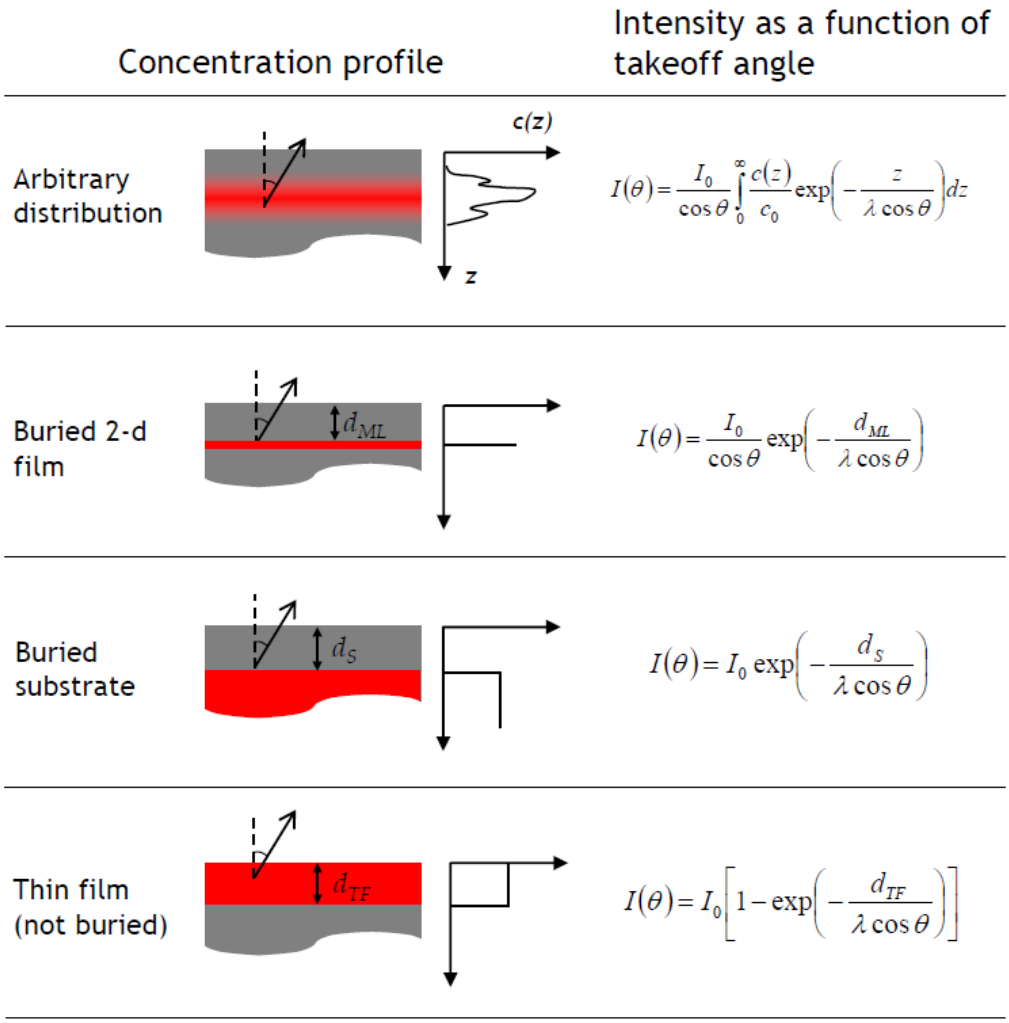

Figure 2.5: Summary of different concentration profiles and the models used to represent the intensity as a function of take-off angle, Huges, 2011 [24].

2.6 Atomic Force Microscopy

Atomic Force Microscopy (AFM, Bruker Innova, tapping mode) was used to examine the topography of the deposited thin film and is located in B40 complex. The tapping mode allows the cantilever to oscillate based on the topography of the sample. The oscillation amplitude changes as interactions (e.g. Van der Waals forces) develops when the tip comes to closer contact with the sample. An electronic servo constantly monitors the amplitude change and maintains the distance between the tip and sample. An AFM image with surface profile is produced by recording and translating the amplitude change as it scans over the sample. AFM data and images are exported and analyzed using Gwyddion software, version 2.55. Horizontal profiles and RMS roughness are reported.

CHAPTER 3

EXPERIMENTAL APPROACH

3.1 TEMAZ/4-Octyne Coadsorption

3.1.1 Sample Preparation

Samples used in the experiment are SiO_2 and Cu. To obtain SiO_2 couple sample, a stripe of SiO_2 is first cleaved from a 300 mm double-side polished, Si(100) wafer (B doped, resistivity 38-63 Ω cm), then 10 x 25 mm^{-2} rectangular sample is diced from the stripe. The as-received wafer has a native oxide layer due to exposure in the atmosphere. To create a so called "chemical oxide" layer, the cleaved sample is taken to Cornell NanoScale Science and Technology Facility (CNF) for further treatment. The sample is dipped in the buffered oxide etch (BOE) solution for 2 minutes to remove native oxide layers. The oxide is formed by dipping the sample in Nanostrip for 15 minutes at 75 °C. The formed "chemical oxide" layer is hydroxylated and 15 - 20 Å thick and corresponds to a surface density of 5 x 10^{14} OH-cm^{-2}. 10 x 25 mm^{-2} rectangular Cu sample is cleaved from a SiO_2 that has 100 nm PVD deposited Cu (Cu—Ta(adhesion layer)—SiO_2) and used as received.

3.1.2 Microreactor Preparation

Microreactor preparation includes reaction zone formation, program setup, and bubbler setup. As discussed in section 2.2, SiO_2 and Cu substrates are clipped on

the sample holder and loaded to the intermediate chamber. The holder is then rotated towards microreactor. With loadlock gate valve shut, the intermediate chamber is in isolated volume. To prevent oil back flows from the downstream mechanical pump, before opening to the reactor, the pressure between intermediate chamber and reactor first needs to reach a comparable level. To do this, a bellow-sealed valve connected to a nitrogen cylinder is open, and 10 sccm of curtain gas (N_2) regulated by a mass flow controller is sent into the intermediate chamber. Once pressurized, the reactor gate valve is open to connect the two sections, and the reactor probe can be transferred to form the reaction zone.

To form the reaction zone, the reactor and the entire panel assembly needs to travel until a contact is formed with the sample holder. The reactor is mounted on a linear motor stage and the motion is controlled by computer aided program. Continuity check is constantly performed while the reactor travels before the reaction zone is formed. A multi-meter is used to check the resistance between the reactor probes and sample holder. Good reaction zone forms when the resistance for four probes is sufficiently low. In the meantime, the heater power is turned up to 9.4%, which anneals the substrate at 150 °C for an hour to remove surface oxide on copper.

Labview program is setup to control the exposure sequence and time. The Labview program controls the exposure by modulating the three-way pneumatic valve assembly located in each delivery channel. The duration for each exposure step is set such that the program executes each step when it is time. Each step has different status for valve opens or closes to direct the flow to either the reactor or mechanical pump.

The TEMAZ bubbler is placed in a water bath and heated to 40 °C to gen-

erate vapor pressure of about 30 mTorr[23]. Because 4-octyne is high in vapor pressure, the bubbler is placed in an ice bath and DI water is added to ensure the surrounding temperature is about 0°C. The delivery lines downstream of the bubblers are also heated using heating tape to eliminate any cold spot at which the precursors might condense.

3.1.3 Growth of ZrO_2 Thin Films on SiO_2 and Cu

ZrO_2 CVD may commence when the substrate temperature reaches the set point, as indicated by the heater. MFCs are first manually turned up to the desired flow rate. The Labview program then executes the MFCs to start the flow, and the directions (to reactor or mechanical pump) are controlled by the three-way pneumatic valve settings. Chemicals are introduced sequentially to the reactor, with co-exposure (4-octyne flows throughout the course of the CVD) "recipe" as following: first, 4-octyne (line C) is introduced to the reactor for 30 seconds. This is to establish a steady-state coverage of co-adsorbate on both substrates, which could also reduce the direct interaction with precursor molecules in the vapor phase. Next, TEMAZ (line A) is introduced for a time period of 2 minutes.O_2 (line B) is then pulsed for variable duration of time. After O_2 pulse, TEMAZ continues to flow for another 25 seconds before it is turned off. 4-octyne continues to flow for another 30 seconds before it is turned off. A complete dosing sequence is summarized in Table 3.1, which include gas flows in each carrier line, the flow rates, as well as the duration for each step.

Figure 3.1(a) shows the dosing diagram, it indicates presence of chemicals as time proceeds. The 4-octyne (green) covers the entire exposure window and

Table 3.1: ZrO_2 CVD Co-exposure Sequence of Dosing

Step	Line A	Line B	Line C	Duration (s)
Co-adsorbate Predose	5 sccm N_2	5 sccm N_2	5 sccm 4-octyne (0 °C)*	30
Co-exposure	5 sccm TEMAZ (40 °C)*	5 sccm N_2	5 sccm 4-octyne (0 °C)	30
Co-reactant Dose	5 sccm TEMAZ (40 °C)	1 sccm O_2 + 4 sccm N_2	5 sccm 4-octyne (0 °C)	2 - 30
Post Co-exposure	5 sccm TEMAZ (40 °C)	5 sccm N_2	5 sccm 4-octyne (0 °C)	25
Purge	5 sccm N_2	5 sccm N_2	5 sccm N_2	30

*TEMAZ and 4-octyne are transported with carrier gas (N_2)

enclosed are TEMAZ (blue) and O_2 (red) doses.

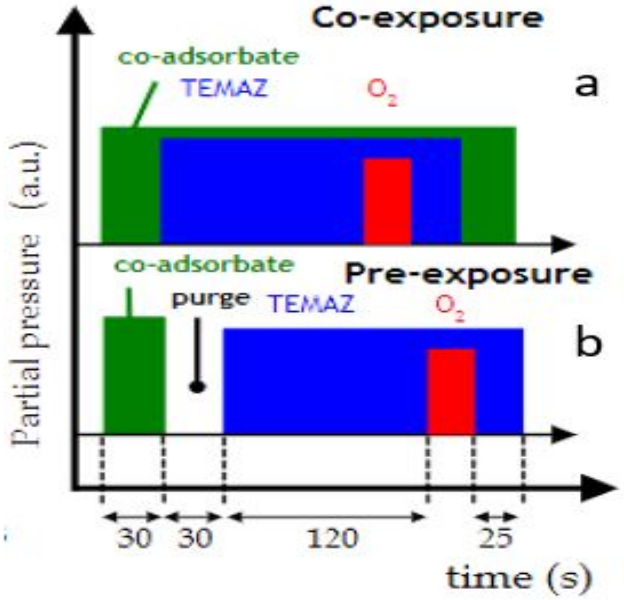

Figure 3.1: Summary of exposure sequence for co-exposure (a) and pre-exposure (b)

3.1.4 Pre vs. Co-exposure Study

It is expected to see thin film growth exclusively on SiO_2 surface, because of strong affinity of 4-octyne towards copper. On the other hand, the chemisorption of 4-octyne on the substrates is a reversible process, making it less likely to be incorporated in the thin film.

To further examine the idea, the pre-exposure (4-octyne is introduced only for a short time period) "recipe" was conducted at the same conditions with substrate temperature of 120 °C and reactor pressure of 1.5 Torr. First, 4-octyne was introduced for 30 seconds and turned off. A stream of purge gas (N_2) was introduced for 30 seconds to remove any remaining 4-octyne. After dosing TEMAZ for 2 minutes, oxygen was introduced for 2 seconds. Finally, when oxygen flow was turned off, TEMAZ continued to flow for another 25 seconds before it was turned off. The dosing sequence is summarized in Table 3.2. Figure 3.1(b) is made to compare with (a) in terms of dosing sequence. The idea is to test whether 4-octyne reversibly binds on the substrates surface at given conditions, or block them permanently. XP spectra for both substrates were analyzed to observe any Zr(3d) peak, AFM image was taken to examine any defect on Cu.

3.1.5 Temperature-Pressure Process Space

The study also aims to explore a process window for this process, as of any other process requiring proper thermodynamics. To investigate the effect of introducing a third species (A) on the nucleation of the precursor (B), a Langmuir model was assumed which includes a set of first-order ordinary differen-

Table 3.2: ZrO_2 CVD Pre-exposure Sequence of Dosing

Step	Line A	Line B	Line C	Duration (s)
Co-adsorbate Predose	5 sccm N_2	5 sccm N_2	5 sccm 4-octyne (0 °C)*	30
Purge	5 sccm N_2	5 sccm N_2	5 sccm N_2	30
Co-exposure	5 sccm TEMAZ (40 °C)*	5 sccm N_2	5 sccm N_2	30
Co-reactant Dose	5 sccm TEMAZ (40 °C)	1 sccm O_2 + 4 sccm N_2	5 sccm N_2	2
Post Co-exposure	5 sccm TEMAZ (40 °C)	5 sccm N_2	5 sccm N_2	25
Purge	5 sccm N_2	5 sccm N_2	5 sccm N_2	30

*TEMAZ and 4-octyne are transported with carrier gas (N_2)

tial equations[20].

$$\frac{d\theta_A}{dt} = \frac{S_A F_A}{n_s}(1 - \theta_A - \theta_B) - k_{d,A}\theta_A \tag{3.1}$$

$$\frac{d\theta_B}{dt} = \frac{S_B F_B}{n_s}(1 - \theta_A - \theta_B)^2 - k_{d,B}{\theta_B}^2 \tag{3.2}$$

The governing equation considers the surface coverage θ_i, the adsorption probability S_i, the impinging flux on the substrate F_i, the surface density of the binding sites n_s, as well as the rate constant of desorption $k_{d,i}$. The above model assumes the adsorptions are spontaneous, while the desorption requires energy barrier. The study found out that at steady-state coverage of the co-adsorbate, increasing substrate temperature will cause decreasing final coverage of the co-adsorbate, and greater partial pressure ratio of the co-adsorbate to the precursor will cause lower final coverage of the precursor.

To visualize the idea, Suh *et al.*[19] predicts the process space exists where

thin film growth occurs only on one surface. The model assumes molecular and reversible binding of the co-adsorbate on the substrate. The plot of the logarithm of the partial pressure of the co-adsorbate versus inverse substrate temperature is shown in Figure 3.2. The slope $\Delta H_{ads,i}/R$ represents the specific selectivity of thin film grows on substrate in the presence of another. The slopes divide the process space into three regions: growth on both surfaces, no growth on either surface, and selective growth on one surface in the presence of another. It demonstrates a selective process space is existed, given proper substrate temperature and co-adsorbate partial pressure.

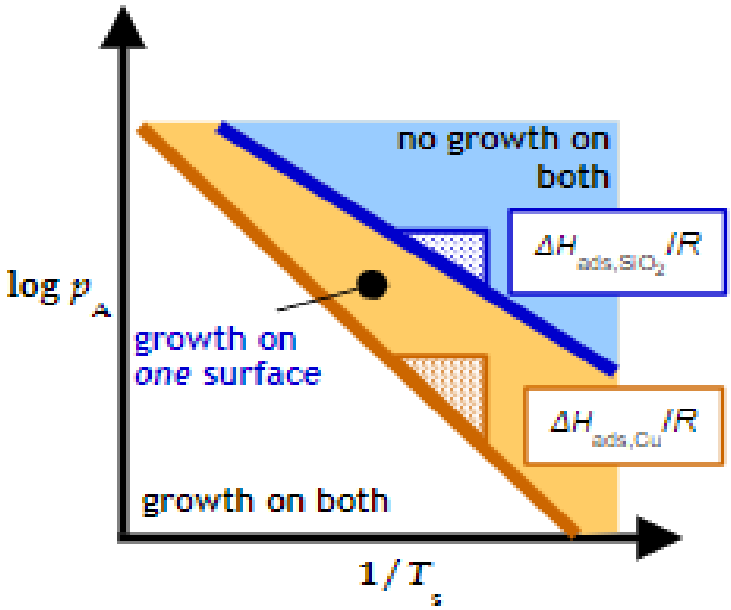

Figure 3.2: Predicted process space in terms of partial pressure of the co-adsorbate and inverse substrate temperature

The substrate temperature window includes 120°C, 180°C, and 240°C. The partial pressure varies from 0.105 to 0.36 Torr, while the partial pressure of TEMAZ is maintained constant at 28 mTorr. Each combination of the temperature and pressure is then conducted to investigate the selective growth window.

For each experiment, 2 s of O_2 exposure was used.

3.1.6 *In-situ* XPS

After deposition, the volume in the intermediate chamber is bypassed to the main chamber and pumped away using turbomolecular pump. Generally, post-exposure XPS is done in the second day but still considered *in-situ* because transferring sample inside the UHV system does not introduce air-break.

As discussed in chapter 2, nonmonochromated Mg Kα and Al Kα X-rays are generated from a twin-anode source operated at 300 W (20 mA emission current x 15 kV anode potential). Emitted electrons are collected and the kinetic energies are measured by the electron energy analyzer. The analyzer is set at aperture 4 and high magnification, which corresponds to 1200 um spot size. The sample is positioned towards the X-ray source at an take-off angles of 38.5°. To take a scan, first, a survey scan is performed to scan over binding energy range from 0 - 1000 eV. In general, characteristic peaks associated with C(1s), O(1s), Zr(3d), N(1s), Si(2p), and Cu(2p) would dominate the spectra. Detailed scan with smaller step size and longer dwell time is conducted for the above characteristic peaks, the detailed scan is repeated twice. All the XPS data is analyzed by Casa XPS software.

3.1.7 AFM

AFM was carried out for various samples to examine surface topography upon exposure to different chemicals, and a standard operating procedure is summa-

rized here for future experiments.

The Bruker Innova AFM tool is seated on an air table to eliminate periodic noise occurred during scanning. It is important to keep the table sturdy when the tool is in operation. To start an AFM experiment, simply turn on the nano drive to initialize the system. Remove the protective cover and turn away the microscope to gain access to the motor stage where the cantilever is mounted. Check to ensure the cantilever is mounted properly and the tip is not worn or damaged. In the event of switching tips, cautions must be taken not to break the cantilever and in-person training for switching tips is strongly encouraged. Carefully unplug the motor stage and place the sample onto the magnets. When putting the stage back, align the three points at the bottom with the locators around the sample surface to ensure accurate positioning. Turn the microscope back facing the sample surface.

With the computer on, start the Nano Drive software to ensure tapping mode is selected and click load experiments. The loaded screens are split into two parts, one is for parameter setup and the other is the real-time video from the microscope. Focus on the sample surface by adjusting the knobs located on sides on the AFM tool. Two small knobs are located on both front and side that can move the microscope in horizontal and vertical direction, respectively. The upper knobs on the side are used to control the focus of the microscope. Given the mirror-like image, a common mistake for new users is focusing on the reflection of the sample. To focus on the real sample, slowly move the microscope in vertical direction to focus on small features (such as defects and debris) available from the microscope video, then move the microscope horizontally back and forth. The real sample surface is located when the small feature moves

along with the microscope. Next, with the video screen on, align the laser on the end of the cantilever. Laser alignment controls are located on the right side of the probe stage that can shift the laser in both horizontal and vertical directions. A good initial alignment should have the laser placed as wide as the cantilever tip. To complete laser alignment, open up the laser alignment (second icon) from parameter window and adjust the detector controls on the left side of the probe stage. The laser is aligned when the central green light is on and the four surrounding red lights are off. Slowly cover up the tool to complete set-up.

With the parameter window up, click the third icon to start cantilever tuning window. Click the play button to tune the cantilever automatically and a bell shaped frequency curve with sharp peak should present. Tuning the cantilever each time before a new experiment is preferred with tapping mode selected. A deviated frequency profile such as rounded frequency peak may indicate the tip is bad and must be replaced. Click the fourth icon to open up the motor stage control, which moves the motor upside down with different speeds. Slowly (CAUTION!) bring the motor stage in close contact with the sample, but not actually touches the surface. Finally, click the fifth icon to engage the tip. A PID loop controls the feedback of the cantilever, an initial set-point can be applied at the left screen of the parameter window to help better engage the tip. A good estimate is one volt less than the real-time feedback value.

Once the tip is engaged, a scanning mode control window will pop open. Click on channels to select the profiles to be reported. Common channels used include height, tapping amplitude, tapping phase, and TM deflection. Other parameters setups include sample/line which sets the resolution of the scan, scan rate that determines the speed at which the tip travels along the surface,

and scan range. Click the camera button to capture the images during scanning, save the data into proper file holders, and click the play button to begin the scanning.

The data on the channels refreshes every time the tip travels back and forth. An easy way to check whether the tip is in good interaction with the sample is by looking at the height profiles. An ideal interaction will produce relatively matched forwards and backwards height profile. As the scanning progresses, click the auto option in each channel to improve the contrast of image and select 2D plane fit from the drop down menu to flatten the surface for better view. Although with the protective cover on, interference should be minimized as small acoustic noise could interrupt the interactions between the tip and the sample. When the scan completes, save the data with proper file name. Withdraw the tip by clicking the withdraw button and slowly move the motor stage up. Retrieve the sample in reverse order and place the motor stage and microscope back in place. Turn off the nano drive and cover up the AFM tool.

CHAPTER 4

RESULTS AND DISCUSSIONS

4.1 TEMAZ/4-Octyne Coadsorption

4.1.1 Growth of ZrO_2 Thin Films on SiO_2 and Cu

Figure 4.1 summarizes the key results from ZrO_2 CVD using 4-octyne as co-adsorbate. The process temperature is 120 °C and the partial pressure of 4-octyne is 0.36 Torr.

Figure 4.1 (a) shows the film thickness results versus O_2 exposure time for films grown on SiO_2 and Cu substrates. It can be noted that film thickness increases linearly with time on SiO_2, whereas the growth on Cu is almost inhibited. The film thickness on SiO_2 was measured by both ex-situ spectroscopic ellipsometry (SE) and *in-situ* XPS, and that on Cu was analyzed by in-situ XPS. The error bars are displayed to estimate the uncertainty of the thickness values. For those error bars that are not visible, it indicates the uncertainties are smaller than the predicted errors. Figure 4.1 (b) depicts the selectivity as a function of oxygen exposure time. For all of the experiments with varying oxygen pulse, the selectivity is always greater than 0.99. Here, the selectivity is quantified as $S_{ASD} = (D_{gs}-D_{ns})/(D_{gs}+D_{ns})$[25], in which D_{gs} is the thin film thickness deposited on the growth surface and D_{ns} is that on the non-growth surface. Figure 4.1 (c) and (d) exhibit thin film quality on SiO_2 from cross-sectional scanning electron microscopy (SEM) and AFM, respectively. Here, the SiO_2 sample was treated with 30 s oxygen exposure. The SEM image indicates that a thick (30 nm) ZrO_2 film

(in green) was formed uniformly on the substrate (in blue). AFM confirmed the deposited film is very smooth with measured RMS roughness of 0.1 nm. Importantly, there is no significant topographic change concerning the scanned area (10 x 10 μm^2) such as varied film thickness or protruding topography. As confirmed in the 1D line scan shown in (e), the surface height varies within 0.2 Å. Concerning impurity incorporation on copper, the AFM results were compared with that from previous Cu sample that has ZrO_2 deposited. Figure 4.2 shows that the AFM tool is capable of detecting defects such as vacancy and pits that are as small as 0.02 μm^2, which confirms that the sample examined here does not possess defects that are larger than this size.

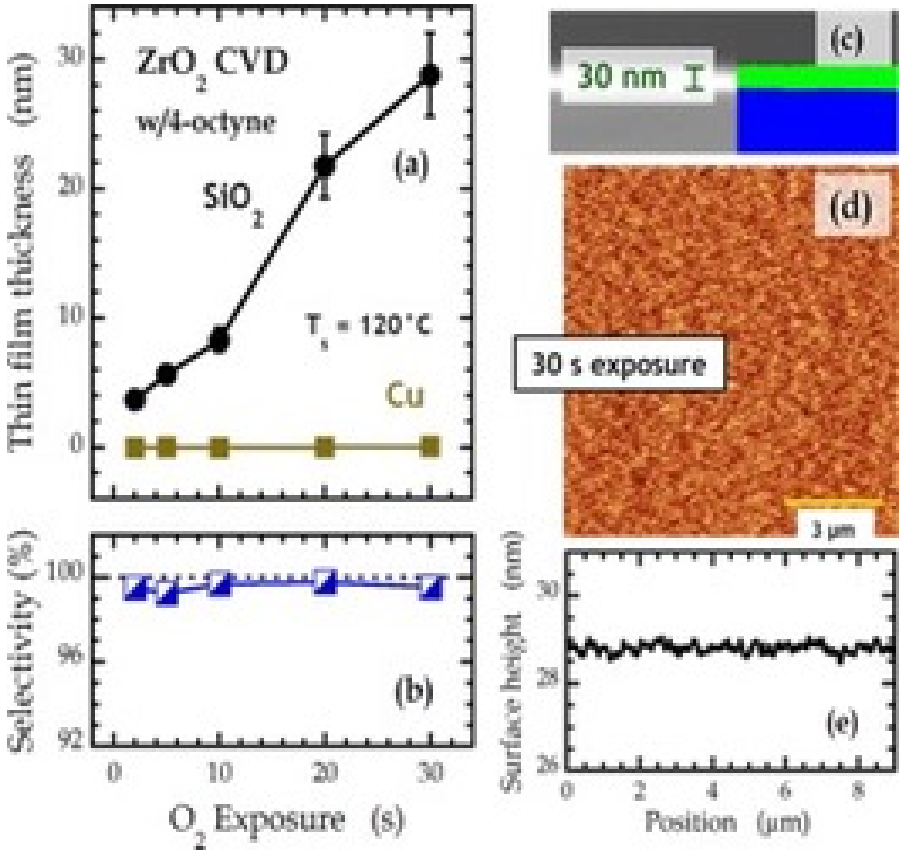

Figure 4.1: Results for ZrO_2 CVD: (a) and (b) film thickness and selectivity plotted against O_2 exposure time; (c) cross-section SEM for thin film grown on SiO_2 at 30s O_2; (d) and (e) AFM image and 1-D line scan for 30s SiO_2

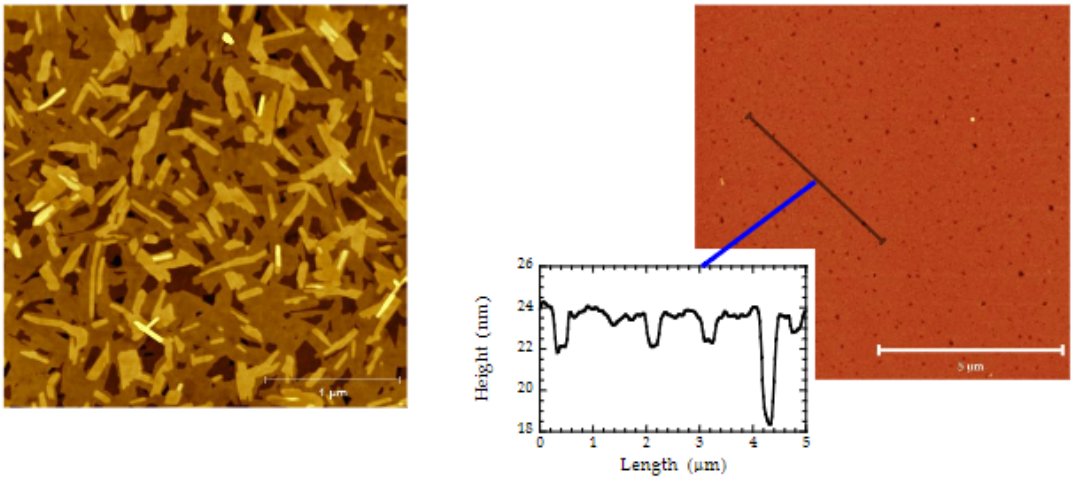

Figure 4.2: Left: AFM scan of an 8 nm thin film, scan area 3x3 μm^2; Right: AFM image of 3 nm ZrO_2 film on Cu, scan area 10x10 μm^2

The experimental results reinforced the theoretical expectations. Collaborators at Distasio research group from Cornell modeled the competitive adsorption mechanism using density functional theory (DFT) calculations[19]. Based on the calculations, it revealed that there is significant binding energetics difference between SiO_2 and Cu upon interacting with 4-octyne. Specifically, the mean value of electronic binding energies (ΔU^{DFT}) for 4-octyne on SiO_2 is -13.58 kcal-mol^{-1}, whereas on Cu is -39.66 kcal-mol^{-1}. It is worth noting that the former is consistent with physisorption of molecules on dielectric surface, whereas the latter possesses more substantial interaction. In fact, the chemical origin of the large energy barrier for 4-octyne on copper results from the rehybridization of the internal C≡C to C=C, upon chemisorbed onto Cu surface. Figure 4.3 summarized the theoretical calculation results. The structural optimizations were performed for three SiO_2 bonding motifs and four Cu binding motifs. As evidenced by the changes in bond length and bond angle, the internal C≡C rehybridizaed to C=C, which is indicative of rehybridization from sp to sp_2 configuration. Recall from earlier discussion, the intrinsic selectivity, which caused

by large enough reactivity between surfaces, is paramount for successful area selective deposition. SiO_2 and Cu represent the combination, in this case, 4-octyne chemiosorbs on the Cu surface while only physisorbed on SiO_2 by weak van der Waals (vdW)/dispersion. The binding of 4-octyne on Cu is more substantial due to this rehybridization of the internal alkyne moiety. Therefore, subsequent CVD process will introduce precursor chemistry primarily on SiO_2 surface, which thin film precursor nucleation is not inhibited by the co-adsorbate.

System	ΔU^{DFT} (kcal-mol^{-1})	ΔH (kcal-mol^{-1})	ΔG (kcal-mol^{-1})	C≡C (Å)	C–C≡C (°)
4-octyne	-	-	-	1.21	178.8
SiO_2 (Binding Motif #1)	-12.06	-11.28	15.79	1.22	177.6
SiO_2 (Binding Motif #2)	-13.71	-12.25	10.89	1.22	175.4
SiO_2 (Binding Motif #3)	-14.96	-15.13	16.76	1.20	174.4
Mean (SiO_2)	**-13.58 ± 1.45**	**-12.89 ± 2.00**	**14.48 ± 3.15**	**1.21 ± 0.01**	**175.8 ± 1.6**
Cu(111) Long Bridge	-39.70	-39.84	-5.92	1.37	126.5
Cu(110) Long Bridge	-35.68	-37.21	-2.88	1.38	123.0
Cu(100) Long Bridge	-42.06	-42.85	-12.46	1.37	125.8
Cu(100) Short Bridge	-41.19	-42.02	-11.23	1.38	124.1
Mean (Cu)	**-39.66 ± 2.83**	**-40.48 ± 2.52**	**-8.12 ± 4.50**	**1.38 ± 0.01**	**124.9 ± 1.6**

Figure 4.3: DFT calculation results for 4-octyne adsorbed on SiO_2 and Cu. ΔU^{DFT}, electronic binding energies; $\Delta H(T,p)$, binding ethalpies; $\Delta G(T,p)$, binding Gibbs free energies; C≡C, triple bond length; and C-C≡C, bond angle

4.1.2 Pre vs. Co-exposure Study

As discussed earlier, the DFT calculations indicate that 4-octyne prefers to bind on Cu surface after which the thin film growth is blocked. However, it is unclear whether the 4-octyne reversibly adsorbs on the surface or forms a permanent blocking layer, which the latter is undesired for ASD. To further investigate the reversibility, the pre-exposure experiment was conducted, and the XPS result is shown in Figure 4.4. The pre-exposure experiment considers the possibility that, in the event of non-reversible adsorption, the adsorbed 4-octyne would have

formed a permanent blocking layer that no film can be grown upon. However, Zr (3d) signals were peaked on both substrates with strong intensity, suggesting that pre-dosing of 4-octyne did not afford selective growth. In addition, SE analysis for SiO_2 samples after both experiments were compared and showed similar thickness (3.5 nm for pre-exposure and 3.8 nm for co-exposure). It confirms that ZrO_2 CVD is not hindered significantly when the co-adsorbate is introduced concurrently. It further demonstrates that chemisorption of 4-octyne is indeed a reversible process and co-exposure is required for this ASD process to exploit the benefits of competitive adsorption.

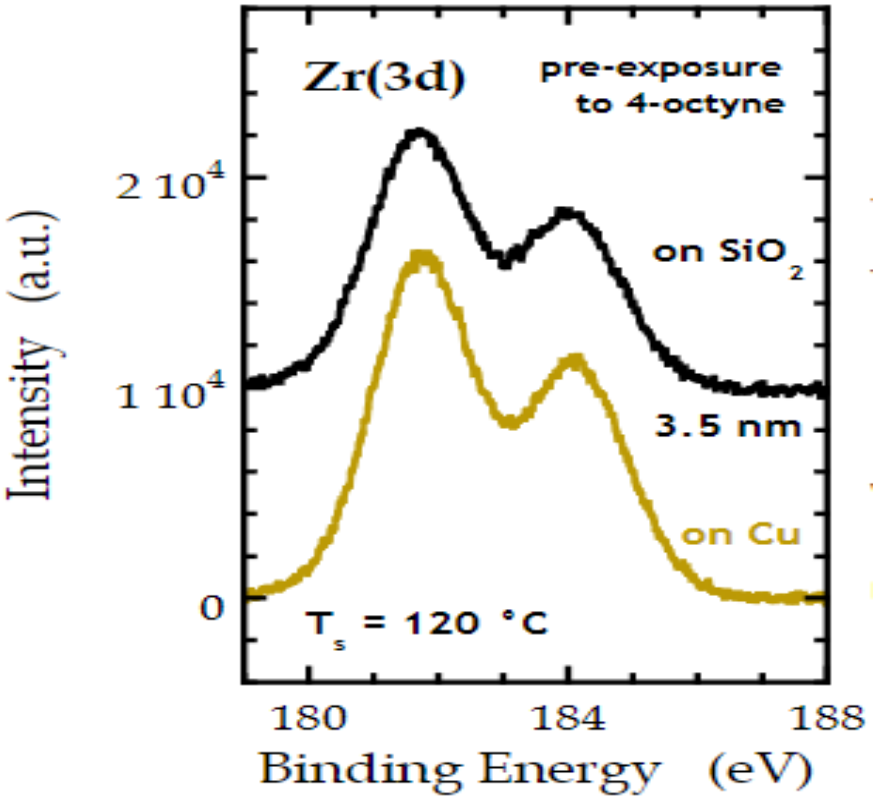

Figure 4.4: XPS result for pre-exposure study, with Zr(3d) signal detected on both substrates

As discussed earlier, the "ABC"-type of ALD introduces a molecular inhibitor to block nucleation on select regions. Although similar to this work,

the "ABC" cycle has separate dosing steps between the inhibitor and precursor, which is equivalent to the pre-exposure study using 4-octyne. The incorporation of unreacted inhibitors in the thin film is detrimental, nevertheless, the blocking on non-growth surface only proceeded up to 15 cycles before noticeable nucleation occurred[17]. On the other hand, the competitive adsorption in our study intentionally introduces precursor and co-adsorbate together to improve dosing efficiency as well as suppressing nucleation on non-growth region.

4.1.3 Temperature-Pressure Process Space

The process phase space was studied for this competitive adsorption mechanism in terms of substrate temperature and co-adsorbate partial pressure. Eight experiment results were summarized in Figure 4.5 and XP spectra are presented for five experiments corresponding to different process conditions. The solid squares represent non-selective depositions and the half-filled squares in blue represent selectivity is realized. For the non-selective growth, significant Zr(3d) peaks are detected on Cu surface, suggesting insufficient coverage of co-adsorbate. Commensurate with the kinetic model for competitive adsorption, it was found an increasing partial pressure of the co-adsorbate and decreasing substrate temperature favored selective growth. In competitive adsorption, the co-adsorbate flux needs to be abundant enough to dominate the binding sites on the substrates. Based on the analytical solution for steady-state coverage of precursor, it is discernible that increased partial pressure of the co-adsorbate (higher F_A) results in reduced coverage of the metal precursor (lower θ_B). On the other hand, too high of the substrate temperature leads to rapid precursor decomposition, which the trends follows Arrhenius relation. In fact, the pre-

cursor TEMAZ starts to decompose as substrate temperature approaching 220 °C [26]. Therefore, the selective deposition is preferred at modest temperature (120 - 180 °C) and high enough vapor pressure such that co-adsorbate is able to suppress precursor adsorption.

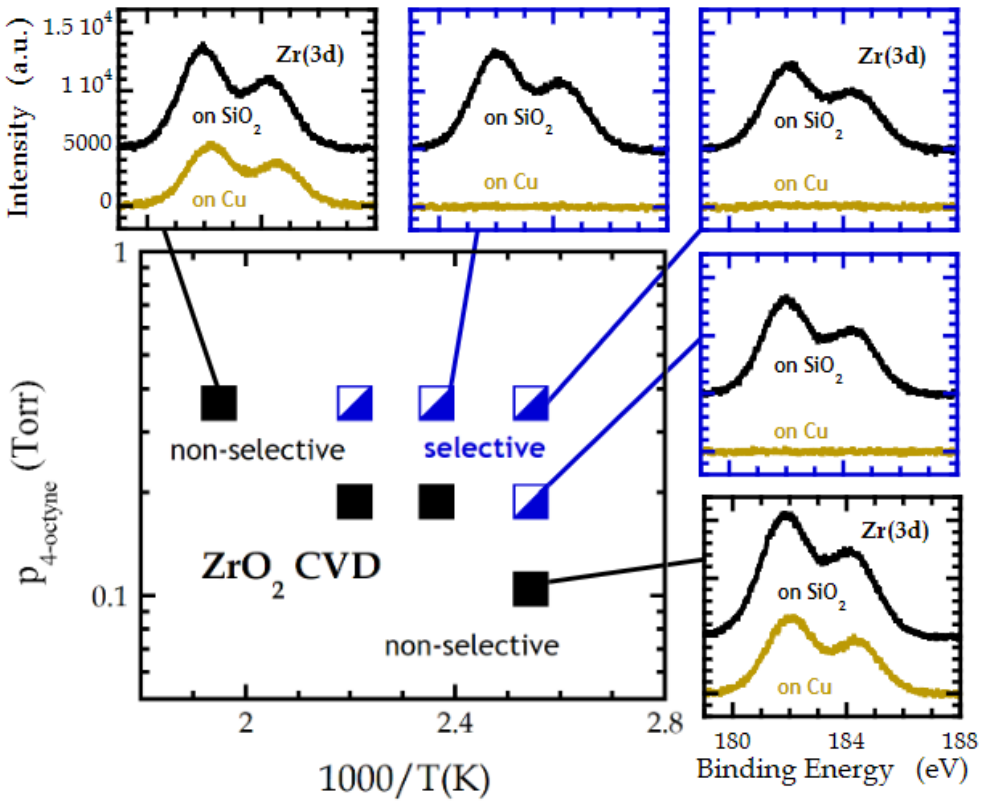

Figure 4.5: Experimental results and XP spectra for ZrO_2 CVD done at various conditions

4.2 Surface Chemistry Study of Cobalt

4.2.1 Considerations for Surface Preparation

As the first trial to demonstrate the versatility of competitive adsorption, cobalt is considered as another substrate candidate. Besides using as a catalyst for Fischer-Tropsch (FT) process to reduce carbon monoxide (CO), cobalt is a promising material to replace copper for local interconnects in future transistor scaling. The major advantage of using cobalt as local interconnect is largely due to its smaller electron mean free path that better fits the nanoscale feature.

The precursor of studying the surface chemistry of any metal is to obtain a clean surface. A single-crystal and contaminant-free cobalt surface is difficult to prepare given the cobalt phase transition temperature is relatively low at about 700 K[27]. Cobalt single crystal exhibits hexagonal closed packed (hcp) structure, and turns to face centered cubic (fcc) structure above this transition temperature. The low transition temperature restricts the use of aggressive annealing to remove surface contaminants, in contrast to other catalyst counterparts, such as Fe and Ru. One of the drawbacks of annealing cobalt single crystal at high temperature is it leads to rapid carbon segregation at the cobalt surface. Hamilton and Blakely found a step change of the annealing temperature from 750 °C to 710 °C induced comparable amount of carbon to cobalt from the minimum level[28], as evidenced by Auger electron spectroscopy.

In response to the challenges brought by aggressive annealing, researchers turned to other methods to produce a clean cobalt surface. The sputter-anneal-cycles of cleaning is one of the generic approaches adopted from Albert *et al.*,

and has been widely used for researchers to explore surface chemistry on clean cobalt surface [29]. The Co(0001) crystal was first sputtered under Ar^+ and subsequently annealed in oxygen environment at 350 °C. The method left carbon and oxygen as major impurities upon cleaning. The sputtered cobalt surface contained carbon equivalent to 1% of a monolayer. Oxygen incorporation was first reduced but became prominent again with continuously increased oxygen exposure. The authors argued the adsorbed oxygen is not at the surface and small concentrations did not affect the following adsorption studies on their cleaned cobalt surface. Studies on oxygen coverage on cobalt indicate that while chemiorosbed oxygen layer is associated with low oxygen exposure, higher exposure leads to cobalt oxide formations. Nevertheless, the method requires one to determine an steady state at which the level of incorporated oxygen is under tolerance. In the context of using cobalt as an alternative substrate in a modified CVD, the adsorbed oxygen level should be minimized.

In fact, the last trace of the oxygen could be removed by annealing in a hydrogen atmosphere, a method fostered by Freund and Hohlneicher [30]. After sputtering, the cobalt sample was annealed in hydrogen and resulted no detectable oxygen level on the cobalt surface while preserving the hcp structure. Other variations include cycles of annealing in UHV or under low pressure of H_2 [31]. Following this procedure, oxygen level can be further reduced to 1-2% of a monolayer. Overall, a generic way to prepare a cobalt surface involves cycles of sputtering under Ar^+ (1-3 kV) at temperature about 350 °C followed by cycles of annealing, preferably under hydrogen to reduce the adsorbed atomic oxygen. The key is to keep the processing temperature under the phase transition window, if the interest is to preserve the hcp structure of cobalt.

4.2.2 Adsorption on Clean Cobalt Surface

There are many potential interactions on cobalt surface in the course of competitive adsorption. A well cleaned cobalt substrate under ambient condition is still subject to various gaseous species, such as oxygen, water, and hydrocarbons. Our focus is to evaluate how these relevant species adsorb on or react with clean cobalt surface.

A simple oxidation experiment on clean cobalt surface under room temperature was conducted by Lahtinen *et al.* and the XP spectra of O 1s and Co 2p peak evolution was reported[32]. Concerning cobalt 2p, two peaks at 793 eV and 778 eV were assigned to Co $2p_{1/2}$ and Co $2p_{3/2}$, respectively. The two characteristic peaks were shifted to approximately 794 eV and 778 eV upon oxidation, which implies formation of Co_3O_4[33]. The small peak at 532 ev implies CO coverage prior to dosing oxygen. The prominent O 1s peak at 529.5 ev indicates the formation of transition metal oxides. However, it is not useful to determine the actual oxidation stage of Co solely based on the O 1s peak. The satellite peak at about 803 eV became visible after sufficient dose of oxygen, a unique feature that can be used to estimate the oxidation state. The intensity ratio of this satellite peak to Co $2p_{1/2}$ peak is characteristic, about 80% for CoO and 20-30% for Co_3O_4[33]. It appears that Co_3O_4 forms initially at low oxygen exposure, which subsequently converted to CoO upon annealing *in vacuo* at 700 K. Effect of water vapor on cobalt surface was also analyzed by examining O 1s XP spectra evolution with water exposure, but no significant interaction was found. The initial water vapor interaction on cobalt at 80 K resulted in O 1s peak at 530.5 eV and characterized as surface hydroxyl groups[34]. Water molecularly adsorbed onto Co led to an O 1s peak centered at 532.5 ev, which completely desorbed

upon heating to 295 K, as the O 1s peak centered back to 530.5 eV.

Besides studying oxide formation on cobalt surface, Kizilkaya *et. al* studied atomic oxygen adsorption on clean and defective cobalt surface with no intention to oxidize the surface. Specifically, the oxygen initially adsorbs onto a flat Co(0001) and forms p(2 x 2) adlayer which continuously develops as O_2 exposure increases up to 15 L. The saturated atomic oxygen coverage on cobalt at 250 K was found to be 0.39 of a monolayer before oxide formation commenced. On a defective Co(0001), however, there was about twice as much as adsorbed oxygen adlayers, due to more binding sites available associated with "defective" surface. Subsequent kinetic study confirmed annealing the sample in 2.3 x 10^{-5} mbar H_2 could effectively remove this chemiosorbed oxygen adlayer at temperature above 450 K for flat and 550 K for defective Co(0001), suggesting higher activation energy barrier for water formation on defective cobalt surface.

Hydrocarbon adsorption on cobalt surface is of great interest as the future coadsorption experiments involve 4-octyne interacts with cobalt surface. Although studies are few regarding direct 4-octyne adsorbs on cobalt surface, the bonding of acetylene and ethylene on Co(0001) by Albert *et al.* provided great insights on the adsorption mechanisms. Two important conclusions can be drawn from the study: while acetylene chemisorbed on cobalt surface and remained stable at least 300 K, chemisorbed ethylene completely decomposed below room temperature; the adsorbed acetylene monolayer has no vacant binding sites thus preventing further coadsorption of other species, whereas adsorbed ethylene monolayer has enough vacancy to accommodate coadsorption.

For acetylene, the electron density is donated from the triple bond to the cobalt surface, and from the cobalt d orbital back to the π^* orbital in the hydro-

carbon. The process is described by Dewar-Chatt-Duncanson model that results in the elongated carbon-carbon bond parallel on the surface. Importantly, acetylene adsorption on cobalt causes rehybridization of the hydrocarbon which enables strong bonding to the surface, which is in agreement with our results from 4-octyne on copper. Furthermore, the adsorbed acetylene monolayer does not provide vacant binding sites for other species, which provides great opportunity for studying 4-octyne coadsorption with ALD precursors. Further heating to 600 K did not cause acetylene desorption from the cobalt surface, leaving it as an irreversible process. In order to be functioned as co-adsorbate in competitive adsorption, the molecules need to reversibly adsorb on the surface to avoid incorporating impurities.

Unlike acetylene, ethylene adsorbed on Co(0001) leaves vacant binding sites that can accommodate other species, but began to decompose at 180 K and completely decomposed below room temperature. The generated vacancies are due to the formation of domain boundaries at the metal surface. Importantly, ethylene molecule can occupy a vacant site only if the adjacent four sites are available as well[29]. The rapid decomposition at low temperature can be explained by this bonding prerequisite since enough vacant sites tends to foster decomposition through four C-H bond scissions, which is faster as compared to the usual C-C scission mechanism for acetylene. Regarding ethylene as a co-adsorbate, although the adsorption is reversible, one needs to address the challenge brought by the vacant sites, which in turn contributed from the adsorption mechanism.

4.3 Competitive Adsorption as a Proof-of-Concept Approach

Intrinsic selectivity between substrates are essential to competitive adsorption utilizing a third species. The greater affinity difference towards substrates, the longer nucleation delay is expected. Copper is a Group 11 transition metal which the 3d shell is filled with electrons, therefore, it is less reactive compared to cobalt which is a Group 9 metal. If one were to repeat the same process with cobalt, considerations have to include ways to produce a clean starting surface and reversibility of the co-adsorbate adsorption, among other new interactions.

Likewise, the choice of an ideal co-adsorbate candidate involves evaluating the molecular structure, which in turn determines its transport in vapor phase, bonding interactions on the substrates, and potential side reactions with other gas molecules. The fact that 4-octyne reversibly chemiosorbes on Cu due to re-hybridization of the internal C≡C does not guarantee the same chemistry would occur with another metal. As such, one needs to consider a group of molecules that will selectively bind on one substrate in the presence of another, evaluate and utilize the chemical origin of this affinity difference towards area selective deposition.

The approach is also applicable to ALD, given the correct dosing sequence can be implemented. To pronounce the benefits of competitive adsorption, one could introduce precursor and co-adsorbate moleclues together in the first half-reaction. Given sufficient residence time, the non-growth substrate is ideally covered with monolayer of the co-adsorbate, whereas the growth surface is chemiosorbed by precursor molecules. After the first purge cycle which removes the co-adsorbate, the co-reactant is introduced and reacts with adsorbed

precursor intermediates to form thin film in the second half reaction. The second purge cycle will generate new starting surfaces for the next ALD cycle. Precise thickness control is achieved by layer-by-layer growth. In the ALD process, fewer interactions are associated with introducing co-adsorbate. For example, the potential side reaction between co-adsorbate and co-reactant can be eliminated by the purge step between the half-reactions.

Finally, it will be awarding to see the reverse deposition, selectively depositing thin film on metal in the presence of dielectric substrate. The key is to identify a group of molecules that preferably blocks on dielectric surface. In fact, various SAM layers have been reported capable of deactivating surface hydroxyl groups on oxide underlayers[15]. The aliphatic alkyltrichlorosilanes, for example, replaces the surface hydroxyl group (Si-OH) with covalent Si-O bonds. However, the reversibility of the chemiosorption of the new co-adsorbate needs to be evaluated at various process conditions.

CHAPTER 5

CONCLUSION

In conclusion, we have reviewed several experimental approaches to area selective deposition, and developed a competitive adsorption mechanism that utilizes a small molecule to preferentially passivate the metallic (Cu) surface, while enabling ZrO_2 thin film to grow exclusively on the dielectric substrate (SiO_2). The grown thin film possessed the comparable quality compared to the one afforded by general CVD process (without adding co-adsorbate). The high degree of selectivity can be preserved provided appropriate substrate temperature and co-adsorbate vapor pressure are selected. The process is entirely in vapor phase makes it capable to be integrated into various 'bottom-up' approaches for semiconductor fabrication. For a co-adsorbate candidate, the intrinsic affinity difference towards substrate is crucial, yet the additional interactions with precursor and co-reactant need to be considered as well.

BIBLIOGRAPHY

[1] E. P. DeBenedictis et al. “Sustaining Moore’s law with 3D chips”. In: *Computer* 50.08 (Aug. 2017), pp. 69–73. ISSN: 1558-0814. DOI: 10.1109/MC.2017.3001236.

[2] Xirong Jiang et al. “Application of atomic layer deposition of platinum to solid oxide fuel cells”. In: *Chemistry of materials* 20.12 (2008), pp. 3897–3905.

[3] John H Holtz and Sanford A Asher. “Polymerized colloidal crystal hydrogel films as intelligent chemical sensing materials”. In: *Nature* 389.6653 (1997), pp. 829–832.

[4] Paul V Braun, Stephanie A Rinne, and Florencio Garcıa-Santamarıa. “Introducing defects in 3D photonic crystals: state of the art”. In: *Advanced Materials* 18.20 (2006), pp. 2665–2678.

[5] YI Zhang, Luyao Zhang, and Chongwu Zhou. “Review of chemical vapor deposition of graphene and related applications”. In: *Accounts of chemical research* 46.10 (2013), pp. 2329–2339.

[6] Richard W Johnson, Adam Hultqvist, and Stacey F Bent. “A brief review of atomic layer deposition: from fundamentals to applications”. In: *Materials today* 17.5 (2014), pp. 236–246.

[7] *Atomic Layer Deposition*. https://www.asm.com/technology/key-technologies/atomic-layer-deposition. Accessed: 2020-06-06.

[8] Viljami Pore et al. “Atomic layer deposition of metal tellurides and selenides using alkylsilyl compounds of tellurium and selenium”. In: *Journal of the American Chemical Society* 131.10 (2009), pp. 3478–3480.

[9] ML Green et al. “Nucleation and growth of atomic layer deposited HfO 2 gate dielectric layers on chemical oxide (Si–O–H) and thermal oxide (SiO 2 or Si–O–N) underlayers”. In: *Journal of Applied Physics* 92.12 (2002), pp. 7168–7174.

[10] Stephen McDonnell et al. “Controlling the atomic layer deposition of titanium dioxide on silicon: dependence on surface termination”. In: *The Journal of Physical Chemistry C* 117.39 (2013), pp. 20250–20259.

[11] Rémi Vallat et al. “Selective deposition of Ta2O5 by adding plasma etching super-cycles in plasma enhanced atomic layer deposition steps”. In: *Journal of Vacuum Science & Technology A: Vacuum, Surfaces, and Films* 35.1 (2017), 01B104.

[12] Martijn FJ Vos et al. “Area-selective deposition of Ruthenium by combining atomic layer deposition and selective etching”. In: *Chemistry of Materials* 31.11 (2019), pp. 3878–3882.

[13] Seung Keun Song, Holger Saare, and Gregory N Parsons. “Integrated Isothermal Atomic Layer Deposition/Atomic Layer Etching Supercycles for Area-Selective Deposition of TiO2”. In: *Chemistry of Materials* 31.13 (2019), pp. 4793–4804.

[14] M Yan et al. “Selective-area atomic layer epitaxy growth of ZnO features on soft lithography-patterned substrates”. In: *Applied Physics Letters* 79.11 (2001), pp. 1709–1711.

[15] Xirong Jiang and Stacey F Bent. “Area-selective ALD with soft lithographic methods: using self-assembled monolayers to direct film deposition”. In: *The Journal of Physical Chemistry C* 113.41 (2009), pp. 17613–17625.

[16] Yueming Hua, William P King, and Clifford L Henderson. "Nanopatterning materials using area selective atomic layer deposition in conjunction with thermochemical surface modification via heated AFM cantilever probe lithography". In: *Microelectronic engineering* 85.5-6 (2008), pp. 934–936.

[17] Alfredo Mameli et al. "Area-selective atomic layer deposition of SiO2 using acetylacetone as a chemoselective inhibitor in an ABC-type cycle". In: *ACS nano* 11.9 (2017), pp. 9303–9311.

[18] Elham Mohimi et al. "Area selective CVD of metallic films from molybdenum, iron, and ruthenium carbonyl precursors: Use of ammonia to inhibit nucleation on oxide surfaces". In: *Journal of Vacuum Science & Technology A: Vacuum, Surfaces, and Films* 36.4 (2018), p. 041507.

[19] Taewon Suh et al. "Competitive Adsorption as a Route to Area-Selective Deposition". In: *ACS Applied Materials & Interfaces* 12.8 (2020), pp. 9989–9999.

[20] Jiun-Ruey Chen. "Alternative Routes to Atomic Layer Deposition: Reactor Design and Process Development". PhD thesis. Ithaca NY, 2017.

[21] Suh Taewon. "Study of The Selective Growth of Thin Films: Effects of a Third Species in Atomic Layer Deposition". MA thesis. Ithaca NY, 2017.

[22] Debashis Panda and Tseung-Yuen Tseng. "Growth, dielectric properties, and memory device applications of ZrO2 thin films". In: *Thin Solid Films* 531 (2013), pp. 1–20.

[23] Kevin J Hughes and James R Engstrom. "Nucleation delay in atomic layer deposition on a thin organic layer and the role of reaction thermochem-

istry". In: *Journal of Vacuum Science & Technology A: Vacuum, Surfaces, and Films* 30.1 (2012), 01A102.

[24] Kevin Hughes. "The Initial Stages of Atomic Layer Deposition on Substrates Modified by Organic Thin Films". PhD thesis. Ithaca NY, 2011.

[25] Wayne L Gladfelter. "Selective metalization by chemical vapor deposition". In: *Chemistry of materials* 5.10 (1993), pp. 1372–1388.

[26] Prashant Phatak et al. "Combinatorial tooling for development of cost-effective and efficient ALD". In: *Solid State Technology* 53.6 (2010), pp. 32–35.

[27] Emily A Lewis et al. "Rediscovering cobalt's surface chemistry". In: *Physical Chemistry Chemical Physics* 14.20 (2012), pp. 7215–7224.

[28] JC Hamilton and JM Blakely. "Carbon segregation to single crystal surfaces of Pt, Pd and Co". In: *Surface Science* 91.1 (1980), pp. 199–217.

[29] Mark R Albert, Larry G Sneddon, and EW Plummer. "An UPS study of the chemisorption of acetylene and ethylene on Co (0001)". In: *Surface science* 147.1 (1984), pp. 127–142.

[30] Hans-Joachim Freund and Georg Hohlneicher. "Comparative Study of Adsorbate Systems and Corresponding Compounds Using X-Ray and UV-Photoemission I. Hexagonal (0001) Co/CO, O2 versus Oxides and Carbonyls". In: *Berichte der Bunsengesellschaft für physikalische Chemie* 83.2 (1979), pp. 100–108.

[31] Gerhard A Beitel et al. "A combined in-situ PM-RAIRS and kinetic study of single-crystal cobalt catalysts under synthesis gas at pressures up to 300 mbar". In: *The Journal of Physical Chemistry B* 101.20 (1997), pp. 4035–4043.

[32] J Lahtinen et al. “Adsorption and Desorption Measurements of CO and O2 on Cobalt”. In: *Vacuum* 41.1-3 (1990), pp. 112–114.

[33] RB Moyes and MW Roberts. “Interaction of cobalt with oxygen, water vapor, and carbon monoxide: X-Ray and ultraviolet photoemission studies”. In: *Journal of Catalysis* 49.2 (1977), pp. 216–224.

[34] S Yamamoto et al. “In situ x-ray photoelectron spectroscopy studies of water on metals and oxides at ambient conditions”. In: *Journal of Physics: Condensed Matter* 20.18 (2008), p. 184025.